

Single Edge Collapse Quad-Dominant Mesh Reduction

JULIAN KNOTD, LightSpeed Studios, USA

Mesh reduction using quadric error metrics is the industry standard for producing level-of-detail (LOD) geometry for meshes. Although industry tools produce visually excellent LODs, mesh topology is often ruined during decimation. This is because tools focus on triangle simplification and preserving rendered appearance, whereas artists often produce quad dominant meshes with clean edge topology. Artist created manual LODs preserve both appearance and quad topology. Furthermore, most existing tools for quad decimation only accept pure quad meshes and cannot handle any triangles. The gap between quad and triangular mesh decimation is because they are built on fundamentally different operations, triangle simplification uses single edge collapses, whereas quad decimation requires that entire sets of edges be collapsed atomically. In this work, we demonstrate that single edge collapse can be used to preserve most input quads without degrading geometric quality. Single edge collapse quad preservation is made possible by introducing dihedral-angle weighted quadrics for every edges, allowing optimization to evenly space edges while preserving features. It is further enabled by explicitly ordering edge collapses with nearly equivalent quadric error that preserves quad topology. In addition to quad preservation, we demonstrate that by introducing weights for quadrics on certain edges, our framework can be used to preserve symmetry and joint influences. To demonstrate our approach is suitable for skinned mesh decimation (a key use case of quad meshes), we show that QEM with attributes can preserve joint influences better than prior work. We implement and test our approach on 67 static and 19 animated meshes from Sketchfab. On both static and animated meshes, our approach consistently outperforms prior work with lower Chamfer and Hausdorff distance, while preserving more quad topology.

CCS Concepts: • **Computing methodologies** → **Computer Graphics**.

Additional Key Words and Phrases: Mesh Reduction, Quad Mesh Reduction, Skinned Mesh Reduction

ACM Reference Format:

Julian Knodt. 2024. Single Edge Collapse Quad-Dominant Mesh Reduction. *ACM Trans. Graph.* 1, 1, Article 1 (January 2024), 21 pages.

1 INTRODUCTION

Games rely on mesh simplification to generate multiple levels of detail (LODs) for meshes, so as meshes get further away from the viewer they are substituted with cheaper to render approximations of the original mesh. Mesh simplification reduces the number of triangles in a mesh, and industry implementations are built on Quadric Mesh Reduction [Garland and Heckbert, 1997, 1998, Hoppe, 1999], since it can preserve geometry, UV mappings, vertex normals, skinning weights, and other attributes. Quadric mesh reduction makes it easy to drop automatically generated LODs into rendering pipelines

Author’s address: Julian Knodt, julianknodt@gmail.com, LightSpeed Studios, Bellevue, Washington, USA, 98004.

Permission to make digital or hard copies of all or part of this work for personal or classroom use is granted without fee provided that copies are not made or distributed for profit or commercial advantage and that copies bear this notice and the full citation on the first page. Copyrights for components of this work owned by others than the author(s) must be honored. Abstracting with credit is permitted. To copy otherwise, or republish, to post on servers or to redistribute to lists, requires prior specific permission and/or a fee. Request permissions from permissions@acm.org.

© 2024 Copyright held by the owner/author(s). Publication rights licensed to ACM. 0730-0301/2024/1-ART1 \$15.00
<https://doi.org/>

with little manual modification. There are a plethora of industry tools for producing simplified meshes, including Simplygon [Donya Labs AB, 2022], InstaLOD [Nerurkar, 2021], and tooling within DCC tools such as Blender [Blender Online Community, 2018] and Unreal Engine [Epic Games, 2022]. Unreal Engine in specific contains “Nanite”, a system built on top of QEM, which generates LODs for different patches of a mesh and switches between them at runtime. Due to Unreal Engine’s ubiquity, Nanite is used by many games as a drop-in LOD system. These tools are built-to-purpose and are able to produce *visually* similar meshes but often operate purely on triangle meshes, whereas many artist created meshes are quad-dominant meshes. In addition to visual similarity, artists often want decimation to preserve edge topology and edge loops, as they affect the animation and deformation of the mesh. With that said, current mesh reduction usually destroys the topology of the output mesh, making it uneven and irregular, independent of the input topology quality. Tools that do preserve quad topology, such as quad reduction in Simplygon often operate entirely on quad meshes, making it brittle to use in practice. In contrast, recent proprietary tooling in Electronic Art’s Frostbite Engine [Mason, 2020] supports mixed input quad/triangle meshes, while preserving quad topology and symmetry, simplifying artists’ workflow for manual modification. While EA’s tool is not public, it was described at a GDC talk to be based on Quadrilateral Mesh Simplification [Daniels et al., 2008], with additional modifications that allow partial quad-chords to be decimated, where a quad-chord is a set of conjoined quads such that only adjacent quads share a vertex (See Fig. 2). One key insight from EA’s tool is that artists do not need all quads to be preserved, but ask that *most* will be preserved, relaxing the requirement that all quads be kept. While the presentation of Frostbite’s mesh reduction shows visually pleasing results, from their description it is a complex system with many heuristics and is not easily replicable. Our motivation in this work is driven by asking if there is a simpler approach to preserve topology and quads in mesh reduction.

This leads us to question why triangle mesh reduction currently cannot preserve quad topology, and we identify three key reasons that quads are not preserved with existing mesh reduction techniques. First, the tangent space for each quadric is ill-conditioned, such that vertices output from edge-collapse can lie anywhere in a face’s plane and cannot be distinguished by quadric error. Second, quad meshes and quad-chords contain edges that have nearly equivalent quadric error. Due to floating point error when computing quadrics or negligible but real geometric differences, these edges are treated as geometrically different, which is manifested in the ordering of edge collapses. While the ordering over these equivalent sets of edges is deterministic, it is essentially random, preventing topological preservation for regions where edges have near equivalence. Third, we observe that memoryless simplification discards the constraints of the input mesh, making it difficult to preserve topology.

To remedy these shortcomings, we introduce a number of modifications to quadric mesh reduction. To fix the ill-conditioned tangent

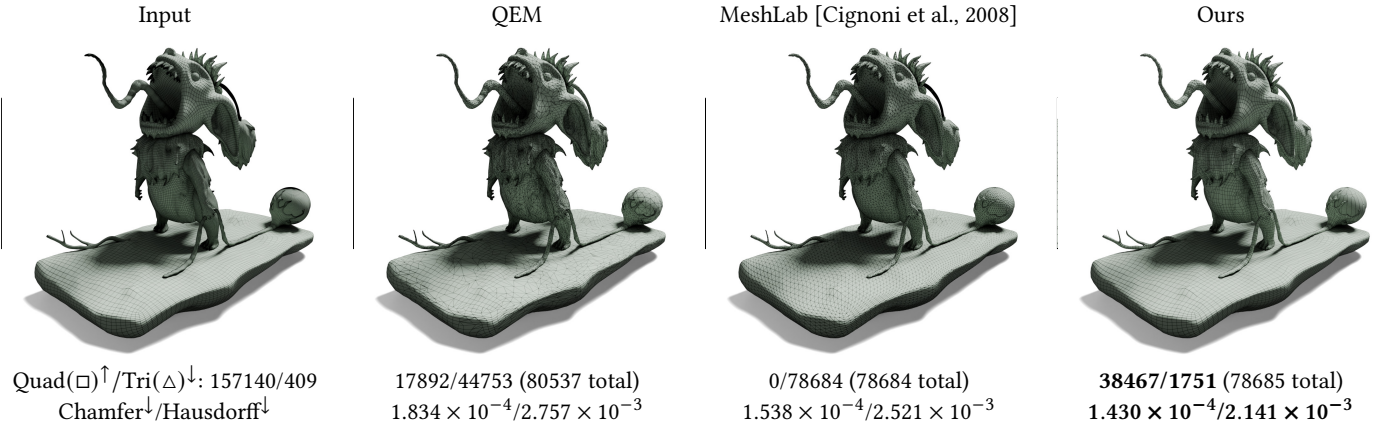


Fig. 1. Our approach is able to better preserve input topology and quads than QEM [Garland and Heckbert, 1997, Hoppe, 1999] for hybrid triangle/quad meshes, with comparable geometric similarity to the input mesh. In the zoomed inset, the input sphere becomes triangulated in QEM and the floor has many high valence vertices, whereas our approach preserves quads on the sphere and floor. We also compare to MeshLab [Cignoni et al., 2008], which requires that the input mesh be triangulated before decimation, making it unsuitable for quad preservation. © Humesh Dilchund.

space of each face, we introduce a per-edge dihedral-angle weighted quadric orthogonal to the adjacent faces' normals. This quadric leads to an even distribution of vertex positions in the tangent space of each face and preserves sharp geometric features. To resolve ambiguity between approximately equivalent edges and to preserve clean topology, we treat edges as having equivalent error if their quadric errors are within some distance, and within sets of equivalent edges we introduce a stateful ordering based on the recency of collapsed opposing quad edges. Finally, we do not perform memoryless simplification, allowing us to preserve all input constraints, but modify the quadric error to represent the error from the current state, rather than the error from initialization. This change serves the same purpose as memoryless simplification, and is equally performant both in runtime and efficacy. An example of the results from our approach are shown in Fig. 1.

Since our approach adds per-edge quadrics, it naturally lends itself to introducing importance weights along each edge, also known as weight painting. To demonstrate how importance weights can be used, we test using per-edge symmetry and joint distance to preserve certain edges more. This stands in contrast to the original QEM, which has no explicit tools to preserve joint regions used in animation, and is unable to preserve edge-loops on key axes of symmetry. Our approach can more easily preserve symmetry and joint regions by measuring a per-edge importance, and increasing the weights of the corresponding quadrics.

To validate that our approach is suitable for joint preservation, it is necessary to show our approach can preserve geometric similarity to the original mesh during skinned animation. While reviewing prior work, we found that while all previous approaches had acknowledged the existence of [Hoppe, 1999], none had tested its ability to preserve joint influences. This is due to the assumption that joint influences are a special attribute which affects geometry unlike other attributes. We test this assumption and directly

use [Hoppe, 1999] to preserve joint influences, and find that it outperforms prior work on articulated mesh simplification, without needing animations or poses.

To demonstrate the proposed improvements, we test our approach on 67 static mixed quad/tri meshes and 19 animated triangle meshes from Sketchfab [Sketchfab, 2022]. Our approach is able to preserve clean quad topology on the tested meshes, while also maintaining geometric fidelity. To measure the geometric quality of the simplified, we measure the Chamfer and Hausdorff distances from the original mesh. To measure the ability to preserve topology, we compare the difference the ratio of the outputs quads to the total number of triangles to the ratio of input quads to the total number of triangles. Our approach has consistently higher or similar geometric quality, while at the same time is able to preserve a significantly higher fraction of input quads.

To summarize, the contributions of this work are as follows:

- (1) An algorithm that adapts single edge-collapse for quad-dominant mesh reduction while still preserving geometric quality. This includes adding per-edge quadrics, revisiting the equation for quadric error, and specially ordering edges with near equivalent quadric error. This approach is validated by thorough testing on a diverse dataset, where it preserves significantly more quads while maintaining high geometric fidelity.
- (2) An extension of per-edge quadrics to demonstrate that our approach supports soft-symmetry preservation along symmetric axes, and can improve joint preservation by increasing weights near key joints.
- (3) A test of [Hoppe, 1999] to show it is suitable for the preservation of joint influences on skeletal meshes.

2 RELATED WORK

Static/Animated Triangular Quadric Mesh Reduction. A large body of work has been devoted to geometry processing using quadrics,

starting from the original quadric mesh reduction algorithm [Garland and Heckbert, 1997]. Quadric mesh reduction was then extended to preserve attributes [Garland and Heckbert, 1998, Hoppe, 1999], where “attributes” are arbitrary variables defined per vertex, which are linearly interpolated using a functional, $\mathbb{R}^3 \rightarrow \mathbb{R}$. Quadrics have also been applied to animated mesh simplification [DeCoro and Rusinkiewicz, 2005, Fuhrmann and Schmalstieg, 1999, Houle and Poulin, 2001, Landreneau and Schaefer, 2009, Shamir and Pascucci, 2001]. In [DeCoro and Rusinkiewicz, 2005], quadrics are computed at multiple poses of the input mesh, and joint influences are computed as linear interpolations between vertices upon collapse. [Landreneau and Schaefer, 2009] takes a different approach, treating joint simplification as an alternating optimization problem over joint weights and vertex position. Outside of articulated mesh simplification, quadrics have been used to generate other simplified representations of meshes, such as sphere meshes [Thierry et al., 2013, 2016], remeshed surfaces [Zhao et al., 2023], simplified Bezier splines [Wang et al., 2023], or with manipulating mass moments [Hafner et al., 2024]. There has also been a recent preprint which examines using a virtual edge-collapse [Liu et al., 2024] and rebaking output textures to a new UV. While this may work well in some cases, such as decimation below 10%, for downstream applications that require multiple levels of detail it is not possible to generate new UVs as different levels of detail rely on texture reuse.

Quadrilateral Mesh Reduction. In parallel to triangle mesh reduction, there has been work in quad-only mesh simplification [Bozzo et al., 2010, Daniels et al., 2008, Tarini et al., 2010], and quad mesh generation [Jakob et al., 2015, Pietroni et al., 2021, Tarini et al., 2011]. Pure quad mesh simplification replaces the edge-collapse operator in triangle mesh reduction with coarser operators such as quad-chord removal, quad diagonal collapses, and single/doublet collapses. This makes current algorithms for quad mesh simplification incompatible with approaches for triangle mesh simplification, despite their facades appearing similar. A downside of pure quad-chord based decimation is that quad-chords are often non-local and may wind around the mesh surface, which, when decimated, may lead to coarse results. To mitigate this coarseness, there is also mixed quad simplification, using partial quad-chord simplification [Mason, 2020]. This approach decimates parts of quad-chords, at the cost of introducing triangles. Since this work is not public, it is unclear their exact criteria for splitting quad-chords, and how many triangles are introduced by quad-chord splitting.

Near Equality with Floating Point Numbers. One key component of this work is comparisons of floating point numbers and their approximation errors, so we briefly describe floating point and their presence in geometric algorithms. Floating point numbers are the most common digital representation of the real numbers. Floating point quantizes the set of real numbers into logarithmically spaced values centered around 0, and all floating point arithmetic maps to this finite set. Since the set is finite and arithmetic operations may not fall exactly on quantized values, arithmetic operations introduce approximation error. Exactly how approximation error is introduced is specified by the IEEE-754 standard [IEEE, 1985], with clearly defined and deterministic rules, making it possible to build algorithms which are aware of and directly handle the error. The primary case

where floating point error becomes a problem and must be handled with care is when floating point numbers are *nearly equivalent*, and their relative ordering matters. This is a common problem in areas such as generating manifold meshes [Cherchi et al., 2020, Wang et al., 2020] and collision detection [Brochu et al., 2012, Wang et al., 2022]. Due to difficulty in mitigating near equivalent ambiguity, floating point error motivates work that uses “rationals” [Hu et al., 2020, 2018, Lévy, 2019, Lévy, 2024] or integer computations [Trettner et al., 2022], but these works often trade correctness for being significantly slower. Instead of relying on more precise formats, this work identifies and gets around floating point error, joining a larger body of research that is aware of floating point error [Björck, 1994, Kahan, 1965, Richard Shewchuk, 1997].

3 METHOD

Our approach is built on quadrics [Garland and Heckbert, 1997, Hoppe, 1999], similar to previous mesh reduction approaches, where we define a quadric, $(\mathbb{R}^3, \mathbb{S}^3) \rightarrow \mathbb{R}^3 \rightarrow \mathbb{R}$, as:

$$\text{Quadric}(p, n)(x) = x^\top (nn^\top)x - 2(n^\top p)x^\top n + (n^\top p)^2 \quad (1)$$

where $p, n \in \mathbb{R}^3$, $n^\top n = 1$, and $x \in \mathbb{R}^3$ is the position that the quadric is evaluated at, which is usually the optimized vertex’s position. In [Trettner and Kobbelt, 2020], this is referred to as a “plane quadric”, but we will simply refer to it as a “quadric”. We also define shorthand for the quadric of a face f as $\text{Quadric}(f) = \text{Quadric}(v, \text{normal}(f))$, where v is any of the vertices of f .

Defining Edge Loops. Within the 3D modeling community, it is common to refer to “edge loops”, a term not frequently used in academic work. Edge loops are sets of edges where at every vertex with degree 4, the two edges in the edge loop have one edge clockwise and one edge counterclockwise between them. At vertices which do not have degree 4, edge loops are terminated. More loosely, it’s a set of connected edges with low amounts of twisting. Under this definition, triangle meshes have almost no edge flow. Edge loops arise naturally from quad meshes with a small number of singularities (vertices which are not degree 4), and are desired because they are more easily animated, and can “replicate muscle structure of the real object” [Raitt and Minter, 1998]. This provides one key motivation for our work, allowing artists to decimate a high-density quad-dominant mesh and animate the lower density mesh. By preserving quad topology in the decimated mesh, the artist’s workflow becomes simpler. A figure showing an edge loop and other terms related to quad topology is shown in Fig. 2.

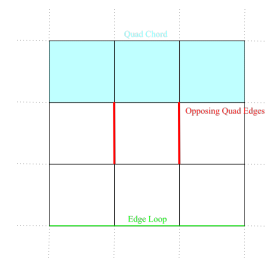


Fig. 2. A visualization of terminology for structure within quad meshes. Part of a quad chord is shown in teal, opposing quad edges are shown in red, and part of an edge loop is shown in green.

3.1 Per-Edge Weighted Quadric

One key reason that clean topology and edge loops are not preserved in QEM [Garland and Heckbert, 1997] is because there are no constraints in the tangent plane of each face. For faces which are coplanar, there is ambiguity where in the tangent plane the collapsed vertex should be placed. To resolve this ambiguity, we introduce additional quadrics in the tangent space of each face. For each edge e with vertices e_0, e_1 and a face f that contains e , we introduce an additional quadric orthogonal to each adjacent faces normal: $Q_{\text{edge}} = \text{Quadric}(e_0, \frac{e_0 - e_1}{\|e_0 - e_1\|_2} \times \text{normal}(f))$, where \times is the cross product. This quadric is weighed according to the dihedral angle if the edge is manifold, or 1 otherwise:

$$w = \begin{cases} \frac{1}{\pi} \arccos(\mathbf{n}(f_0)^\top \mathbf{n}(f_1)) & (e_0, e_1) \in f_0, f_1 \\ 1 & \text{otherwise (edge non-manifold)} \end{cases}$$

$$Q'_{\text{edge}} = w \|e_0 - e_1\|_2 Q_{\text{edge}} \quad (2)$$

where $\mathbf{n}(\cdot)$ is the unit normal of a face, and $\frac{1}{\pi}$ is a normalization constant. In our implementation, we additionally constrain w to $w = \max(w, 1 \times 10^{-2})$ to prevent degenerate quadrics.

By introducing weighted quadrics on each edge, our approach can be used to weigh edges by other attributes. We explore increasing weights on edges by a measure of mesh symmetry across each edge plane, and the distance between joint influences on the end of each edge.

Soft Symmetry. Using the newly introduced per-edge quadrics, we are interested in seeing if they can be used to preserve symmetric topology of the mesh. This is motivated by downstream applications, where some symmetry preservation is often desired as it is easier to manipulate than asymmetric meshes, but not as a hard requirement. To that end, we treat symmetry as an implicit soft constraint, guided by edge collapses. To guide the edge collapses, we increase the weight of each edge's quadrics based on a measure of symmetry across each edge. These per-edge symmetry weights $s \in [0, 1]$ are incorporated by setting w in Eq. 2 as $w = \max(w, \lambda_{\text{sym}} s)$, where λ_{sym} is a parameter that controls the importance of symmetry. To compute s , we compute a matching of all vertices across the plane that spans the edge and the halfway vector between the edges' two adjacent faces for manifold edges, and the singular face's normal for boundary edges. s is then the ratio of vertices that have a matching vertex across the plane within a distance of ϵ_{sym} to the total number of vertices. An example of the weights for each edge and how they are computed is visualized in Fig. 3. This weighting implicitly induces an ordering over edges where edges that are equidistant from the plane of symmetry have equal importance. Pseudocode for our algorithm for symmetry matching is given in the Appendix, Alg. 2.

Preserving Edges Between Distinct Joints. We also use edge weights to more strongly preserve edges with high gradients between joint influences. More plainly, edges where the endpoints have joint influences that are significantly different should be decimated less. For each edge, we compute the difference $d \in [0, 1]$ between joint influence distributions as $\frac{1}{2} \ell_1(j_0, j_1)$, where j_0, j_1 are the discrete set of joint influences at the end of each edge, with each influence

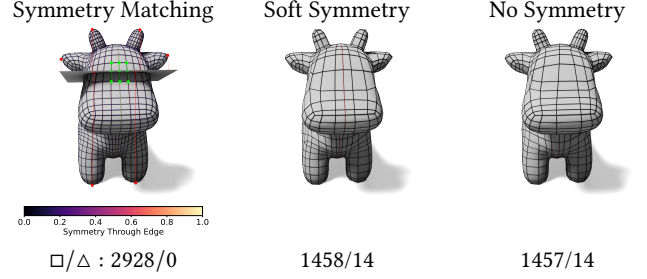


Fig. 3. To measure the symmetry of each edge, we compute a matching of all vertices across the plane that spans each manifold edge and the halfway vector between its two adjacent faces. Left: vertices with a matching are shown in green, and those without are shown in red. Each edge's weight is the fraction of all vertices with a matching. This weight is then used during edge collapse for each edge's quadric. In the middle figure, edges along the axes of symmetry (shown in red) are preserved with this weighting, but are lost when it is not explicitly included, shown on the right. ©Keenan Crane.

$j_{ik} \in [0, 1]$, and $\sum_k j_{ik} = 1$. An example of the ℓ_1 difference between two joint distributions with 2 bone influences each is shown in Eq. 3. We then take $w = \max(w, \lambda_{\text{joint}} d)$, where λ_{joint} is a parameter that controls the importance of joint differences. A visualization of regions where joint influences vary is shown in Fig. 4. Key joint regions such as elbows and fingers have the largest difference, and our decimation allows for controlling how strongly those regions are preserved.

Example ℓ_1 diff. of two arbitrary joint influences: (3)

$$d_{\text{joint}}(j_0, j_1) = \frac{1}{2} \ell_1 \left(\begin{aligned} j_0 : k &= \begin{bmatrix} a & b \end{bmatrix}, j_{0k} = \begin{bmatrix} \alpha & 1 - \alpha \end{bmatrix}, \\ j_1 : k &= \begin{bmatrix} b & c \end{bmatrix}, j_{1k} = \begin{bmatrix} \beta & 1 - \beta \end{bmatrix} \end{aligned} \right) = \frac{1}{2} (|\alpha| + |(1 - \alpha) - \beta| + |-(1 - \beta)|)$$

3.2 Ordering Approximately Equal Edges

Total Ordering. The second key aspect of our approach that allows for preserving quads is that the order of edge collapses is not dictated by quadric error alone. The observation that lead us to modify the ordering is that prior quadric mesh reduction imposes a strict total ordering over all edge collapses. A total ordering is where every element of a set is either greater than, equal to, or less than other elements, and there is no ambiguity in pairwise relationships. This is in contrast to a partial ordering, where some elements are incomparable. For quadric mesh reduction [Garland and Heckbert, 1997], there is an implicit assumption that quadric edge costs exactly and correctly dictate the order of edge collapses. While this makes sense assuming that geometric errors are correct and exact, we reject this assumption because it overly constrains the ordering of collapsed edges with edges that have approximately equal error. As an example, consider the input cube mesh in Fig. 5. Each edge on the

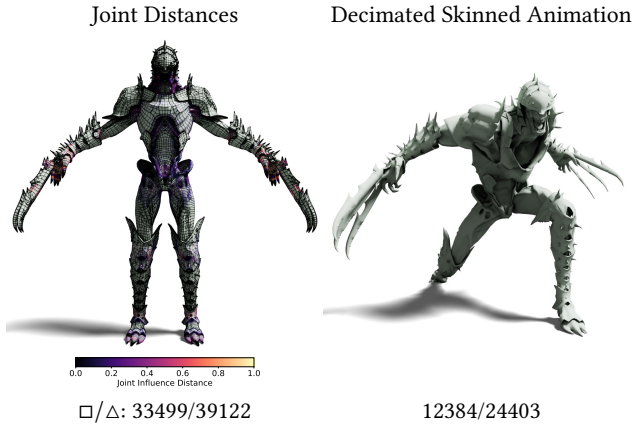


Fig. 4. Left: mesh in its rest pose, with edges marked with higher joint distances highlighted. Most distances are centered around anatomical joints, such as elbows and fingers. Right: frame of the animation of the mesh, visualizing range of motion after decimation. Animations tend to deform regions where joint influences vary heavily between vertices. © 2019 Catholomew.

cube has equal quadric error, with edges periodically spaced along the surface. With floating point approximation though, the ordering of edges is dominated by floating point error. This effectively means the ordering of equivalent edges is deterministically random, and by collapsing these equivalent edges in random order the input topology is destroyed. While floating point error is one motivation of our approach, exact computation will not resolve this problem for two reasons. First, even if edges are found to be exactly equivalent, the ordering over these equivalent edges is unspecified. Second, there may be some real but *negligible* geometric difference between quadric error of edges, which is acceptable to ignore if it helps maintain quad topology. We address this by treating each quadric error as an approximation, and induce a *partial ordering* over quadric errors, treating them as incomparable if they are too close.

Partial Ordering over Edges. We treat comparisons between quadric errors as a partial ordering, where if two edges are compared to be approximately equal we consider it to be indeterminable if one is greater than the other. We define approximate equality between two quadric errors as:

$$a \approx b := |a - b| < \epsilon_{\text{abs}} \quad (4)$$

where ϵ_{abs} is a positive threshold for defining equality based on the difference of the two floats [Dawson, 2012]. The set of collapsible edges is divided into “equivalence classes”, or sets of edges which are approximately equal to each other. Within each equivalence class, we introduce an additional ordering on top of the quadric error, and use an ordering that prefers decimating quad chords. By using such an ordering, quads within each equivalence class are preserved. This approach allows itself to tune the trade-off between quad and triangle preservation by modifying ϵ_{abs} . Since ϵ_{abs} determines whether two edges are considered equal, a higher ϵ_{abs} preserves more quads at the cost of lower geometric similarity, and vice-versa when lowering ϵ_{abs} .

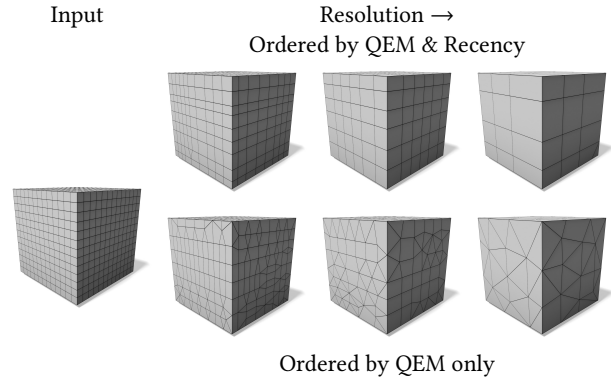


Fig. 5. Cube mesh simplified with our approach. All edges in the input cube have equivalent cost, but differ slightly when computed due to floating point error. We group these approximately equivalent edges and provide an explicit ordering based on the recency of collapsed opposing quad edges, which preserves topology. This is in contrast to ordering purely based on QEM, which is unable to preserve topology.

Ordering Approximately Equal Edge Collapses. For approximately equal edge collapses, we introduce additional state that implicitly collapses quad chords. Specifically, we introduce a metric we call “recency” to determine collapse order. For every edge collapsed, we increase the recency of any edges on the opposite side of quads containing the collapsed edge to the recency of the collapsed edge plus one. A visualization of recency is shown in Fig. 6. We prioritize edges within each equivalence class so that the edge with highest recency is collapsed first. Since opposing quad edges will have higher recency and be collapsed earlier, this leads to an implicit decimation of quad chords. Once an entire set of approximately equivalent edges has been decimated, we reset the recency of all edges to 0, since there is no longer a preference of which edge to decimate.

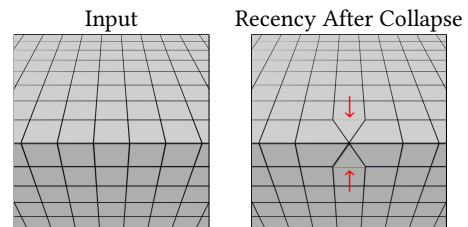


Fig. 6. Before edge collapses, all edges have 0 recency (marked in black). After an edge collapse, opposing quad edges have their recency increased (marked in white with red arrows) by the recency of the collapsed edge plus 1.

Implementation. In our implementation, partial ordering and recency are implemented using two priority queues. The first priority queue is ordered entirely by quadric error, identical to prior approaches (line 14, Alg. 1). The second priority queue is ordered by recency, and if all edges have equivalent recency then it is ordered by quadric error (line 18, Alg. 1). If the second priority queue is empty, one edge is removed from the first priority queue, and

moved into the second priority, with recency 0 (line 17-18, Alg. 1). While the second priority queue is not empty, the highest priority edge is removed from the second priority queue and that edge is collapsed (line 19-21, Alg. 1). For every collapse from the second priority queue, we check if there are edges on the top of the first priority queue which are roughly equivalent, and move them from the first to the second priority queue as long as the top is approximately equivalent (line 25-27, Alg. 1). If an edge has its quadric error updated and it is in the second priority queue, it is moved back to the first priority queue (encapsulated in line 24, Alg.1). The full algorithm of our approach, including updating recency and selecting edges based on priority is in Alg. 1.

Algorithm 1 Quad mesh preserving QEM

Input: vertices V , faces F
Output: new vertices V' , new faces $F' \subseteq F$

```

1:  $Q_i = \text{Quadric}(0)$   $\triangleright$  Initialize zero quadric for all vertices
2: for  $v \in V$  do
3:   for  $f \in F$  if  $v \in f$  do
4:      $Q_v += \text{area}(f)\text{Quadric}(f)$   $\triangleright$  Add quadric for adj. faces
5: for  $(e_0, e_1) \in \text{uniq}(\text{edges})$  do
6:   if  $(e_0, e_1)$  adjacent to  $f_0, f_1$  then
7:      $\angle(e_0, e_1) = \frac{1}{\pi} \arccos(n(f_0)^\top n(f_1))$   $\triangleright$  Manifold Edges
8:   else  $\angle(e_0, e_1) = 1$   $\triangleright$  Non-manifold edges
9:      $w = \max(\lambda_{\text{sym}} w_{\text{sym}}, \lambda_j w_{\text{joint}}, \angle(e_0, e_1), 1 \times 10^{-2})$ 
10:     $Q_{e_0} += w \|e_0 - e_1\|_2 \text{Quadric}(e_0, e_1)$ 
11:     $Q_{e_1} += w \|e_0 - e_1\|_2 \text{Quadric}(e_0, e_1)$ 
12:  $\text{pq}_{\text{qem}}$ : Priority Queue,  $\text{pq}_{\approx}$ : Priority Queue
13: for  $(e_0, e_1) \in E$  do  $\triangleright$  Initialize Priority Queue
14:    $\text{pq}_{\text{qem}}.\text{push}(\text{priority} = \text{CollapseCost}(Q_{e_0}, Q_{e_1}), e)$ 
15: while  $\text{tri count} > \text{target}$  do
16:    $\forall e : \text{Recency}(e) = 0$   $\triangleright$  Reset all recencies
17:    $[\text{qem}, e] = \text{pq}_{\text{qem}}.\text{pop}()$ 
18:    $\text{pq}_{\approx}.\text{push}(\text{priority}=(0, \text{qem}), e)$ 
19:   while not empty( $\text{pq}_{\approx}$ ) do
20:      $[\text{rec}_e, \text{qem}, e] = \text{pq}_{\approx}.\text{pop}()$ 
21:     CollapseEdge( $e$ )  $\triangleright$  Identical collapse to QEM
22:     for  $(e_0^*, e_1^*)$  opposite to  $e$  in any quad do
23:        $\text{Recency}((e_0^*, e_1^*)) += \text{rec}_e + 1$ 
24:     Update one-ring costs and two-ring recency
25:     while len( $\text{pq}_{\text{qem}}$ )  $> 0$  and top( $\text{pq}_{\text{qem}}$ ).prio  $\approx$  prio do
26:        $[\text{qem}_n, e_n] = \text{pq}_{\text{qem}}.\text{pop}()$ 
27:        $\text{pq}_{\approx}.\text{push}(\text{priority}=(\text{recency}(e_n), \text{qem}_n), e_n)$ 

```

This precise ordering relies on *not using memoryless simplification*, and computing all quadrics during initialization. This is because memoryless simplification affects the 2-ring of each vertex, which causes the costs of opposing edges on a quad to change and removes them from the equivalence class. While it was shown in prior work that memoryless simplification leads to improved results, we are able to remove memory simplification and modify the quadric error metric without impacting the geometric quality of our results.

Minimizing Introduced Error. To replace memoryless simplification, we change the QEM error so it no longer measures the error from the initial mesh, but from the decimated mesh. To measure introduced error, we redefine quadric error using the following definition:

$$\text{QEM}(e, v) = (Q_{e_0} + Q_{e_1})(v) - (Q_{e_0}(e_0) + Q_{e_1}(e_1)) \quad (5)$$

Where $v \in \mathbb{R}^3$ is the position of the new vertex, and Q_{e_0}, Q_{e_1} are the quadrics for e_0, e_1 respectively. The first term $(Q_{e_0} + Q_{e_1})(v)$ is the original quadric error metric, and the new term $-(Q_{e_0}(e_0) + Q_{e_1}(e_1))$ is the sum of the current quadric errors of the edge's two endpoints. Using this definition, edge collapses which introduced errors previously will not be penalized if future edge collapses will not introduce additional error. This is similar to using memoryless simplification, since both measure error from the *current* state, rather than from initialization. Since this modification was never mentioned in prior work, it is likely a key reason that memoryless simplification was purported to work better.

Skinned Mesh Reduction. Since quad meshes are crucial to animations and skinning, we also implement animated mesh reduction. There are two prior works we focus on for animated mesh reduction: [DeCoro and Rusinkiewicz, 2005] and [Landreneau and Schaefer, 2009]. Both of these works argue that [Hoppe, 1999] is insufficient for producing high quality joint weights and treat joint influences differently from UVs, normals, and vertex colors. Unfortunately, neither of those works provide evidence that this is true. For our implementation, we adapt [Hoppe, 1999] for joint influence simplification. We treat joint influences identically to other attributes and store a linear functional for each joint influence:

$$j_{ib}(p) = g_{ji}^\top p + d_{ji} \quad (6)$$

Where j_i is the i^{th} joint influence and i goes up to the number of bones, $p \in \mathbb{R}^3$ is the new vertex position, and g_{ji}, d_{ji} are computed identically to other attributes from [Hoppe, 1999]. Since joint influences are sparse, we only store non-zero joint influences of each vertex. To ensure that our quadrics are purely stack allocated (which improves performance), we store a maximum of 16 joint influences per vertex, and if there are more than that we drop the influence with the minimum weight: $\max(g_{ji}^\top p_0 + d_{ji}, g_{ji}^\top p_1 + d_{ji})$, where p_0, p_1 are the positions of the two quadrics being combined. Note that this resolving which vertex to keep only occurs at an extreme decimation when the new mesh does not appear close to the original, and does not occur in our dataset. After decimation, we are able to recover joint influences for all bones that influence any of the merged vertices, and we select the top 4 and normalize their influences to sum to 1. This approach, as compared to [Landreneau and Schaefer, 2009], is independent of the order of collapses, so bone influences will not be culled until the mesh is fully decimated.

Attribute Preserving QEM for Polygonal faces. While [Hoppe, 1999] was designed specifically for triangle meshes, their approach generalizes to faces with an arbitrary number of vertices. This is done by

computing the least squares solution for g, d in:

$$\operatorname{argmin}_{g,d} \begin{bmatrix} p_1^\top & 1 \\ p_2^\top & 1 \\ \cdots & \cdots \\ p_n^\top & 1 \\ n^\top & 0 \end{bmatrix} \begin{bmatrix} g \\ d \end{bmatrix} - \begin{bmatrix} s_1 \\ s_2 \\ \cdots \\ s_n \\ 0 \end{bmatrix} \quad (7)$$

where p_\bullet is the position of each vertex, s_\bullet is the attribute of the corresponding vertex and g, d are terms from the linear functional that determines the attribute at an arbitrary position $s(p) = g^\top p + d$. For our implementation, we use a least squares QR solver to compute g and d .

4 EXPERIMENTS

To test our approach, we gather a dataset of 67 static meshes and 19 animated meshes from Sketchfab [Sketchfab, 2022] containing UV charts, linearly skinned animations, and per-vertex normals. There is a wide diversity of meshes: some pure quad meshes, some pure triangle meshes, and some hybrid meshes. Full statistics for input meshes are shown in the Appendix, Tab. 3. We take care to respect the licensing of the artists, and note that our approach is *not generative AI*, as some artists specifically label their art to not be included for training of generative AI.

We compare our approach to internal tooling used for decimation of meshes, labeled “QEM” in figures. This tool is a battle-tested implementation of [Hoppe, 1999] and [Landreneau and Schaefer, 2009], with additional constraints to prevent degeneracies, and has been used for skinned and static meshes in downstream projects. It can preserve quads by triangulating immediately before decimation and labeling the introduced edges. After decimation, if any of the original labeled edges added during triangulation remain, they are removed and the quads recovered. We also compare to MeshLab’s quadric decimation [Cignoni et al., 2008] which implements [Hoppe, 1999]. [Cignoni et al., 2008] only works for pure triangle meshes and is unable to preserve joint influences, so we only test it on static meshes. In our experiments we compare each approach at triangle ratios of 50%, 25%, and 10%, where triangle ratios are the number of the triangles in a triangulated version of the mesh. We do not compare against any pure quad decimation approach, as such an approach **would not work** on a large subset of our data, and there are no free, canonical, “compiles & works out-of-the-box” implementations.

All animated meshes are in the GLB file format, which only supports triangles and no quads or polygons. Thus, we only compare geometric quality for those meshes, and do not compare quad preservation. MeshLab currently does not support animated mesh decimation, so we only compare QEM, which implements [Landreneau and Schaefer, 2009]. We are shoehorned into using the GLB file format since it is an open standard and has widespread, proper support. Other animated mesh formats such as FBX often introduce subtle bugs due to their closed source, closed specification, and are designed to work within a closed ecosystem. For experiments with animated meshes, we also target triangle ratios of 50%, 25% and 10%. In our experiments we fix $\lambda_{\text{joint}} = 1$, $\lambda_{\text{sym}} = 0$, $\epsilon_{\text{abs}} = 5 \times 10^{-6}$. We ablate λ_{joint} and ϵ_{abs} later in Sec.6.4. We set $\lambda_{\text{sym}} = 0$ and do not

compute symmetric matchings since we assume that the majority of input meshes do not have symmetry.

Through our experiments we demonstrate a few properties:

- (1) Our approach can preserve at least 30% more quads than the baseline during decimation, measured by the ratio of output quads and triangles
- (2) Our approach has higher geometric similarity than prior work as measured by the average Chamfer and Hausdorff distance across the entire dataset.
- (3) Our approach can softly preserve topological extrinsic symmetry in meshes, measured qualitatively on a subset of meshes with symmetry.
- (4) Using [Hoppe, 1999] we are able to preserve animation quality better across animations as compared to [Landreneau and Schaefer, 2009].

All experiments are run on an AMD Ryzen Threadripper 3970X 32-Core CPU without any GPU usage. QEM, MeshLab [Cignoni et al., 2008] and our approach are single-threaded.

5 RESULTS

Static Mesh Geometric Summary Stats

Metric	Ours	QEM	MeshLab
50% Δ			
Avg. Chamfer \downarrow	1.775×10^{-4}	2.881×10^{-4}	2.661×10^{-4}
Avg. Hausdorff \downarrow	7.692×10^{-3}	6.081×10^{-3}	4.977×10^{-3}
Med. $\frac{\text{Out Quads}}{\text{Out Tris}} / \frac{\text{In Quads}}{\text{In Tris}} \uparrow$	0.949	0.674	×
25% Δ			
Avg. Chamfer \downarrow	5.830×10^{-4}	7.950×10^{-4}	9.485×10^{-4}
Avg. Hausdorff \downarrow	1.067×10^{-2}	1.069×10^{-2}	1.221×10^{-2}
Med. $\frac{\text{Out Quads}}{\text{Out Tris}} / \frac{\text{In Quads}}{\text{In Tris}} \uparrow$	0.761	0.437	×
10% Δ			
Avg. Chamfer \downarrow	1.811×10^{-3}	2.066×10^{-3}	3.160×10^{-3}
Avg. Hausdorff \downarrow	1.970×10^{-2}	2.135×10^{-2}	2.366×10^{-2}
Med. $\frac{\text{Out Quads}}{\text{Out Tris}} / \frac{\text{In Quads}}{\text{In Tris}} \uparrow$	0.622	0.256	×

Table 1. Comparison of our approach to an implementation of QEM and MeshLab [Cignoni et al., 2008]. Our approach has better geometric similarity to the original mesh, while also retaining more quads on median. MeshLab requires that the input mesh be fully triangulated and thus cannot preserve any quads.

Quantitative. We compare our results to QEM and [Cignoni et al., 2008] on all static meshes. Summary statistics for our approach are shown in Tab. 1, which shows our approach has comparable or better Chamfer and Hausdorff distance to the baseline approaches while consistently retaining about 30% more quads. [Cignoni et al., 2008] requires that the input mesh be triangulated and because of that is unable to preserve any quads. To visualize the distribution of geometric differences versus topology preservation, we plot the geometric quality against quad preservation of QEM and our approach in Fig. 9, with outliers for both approaches removed from the visualization. Being further right on this chart indicates that the input has more quads, while being further down indicates higher

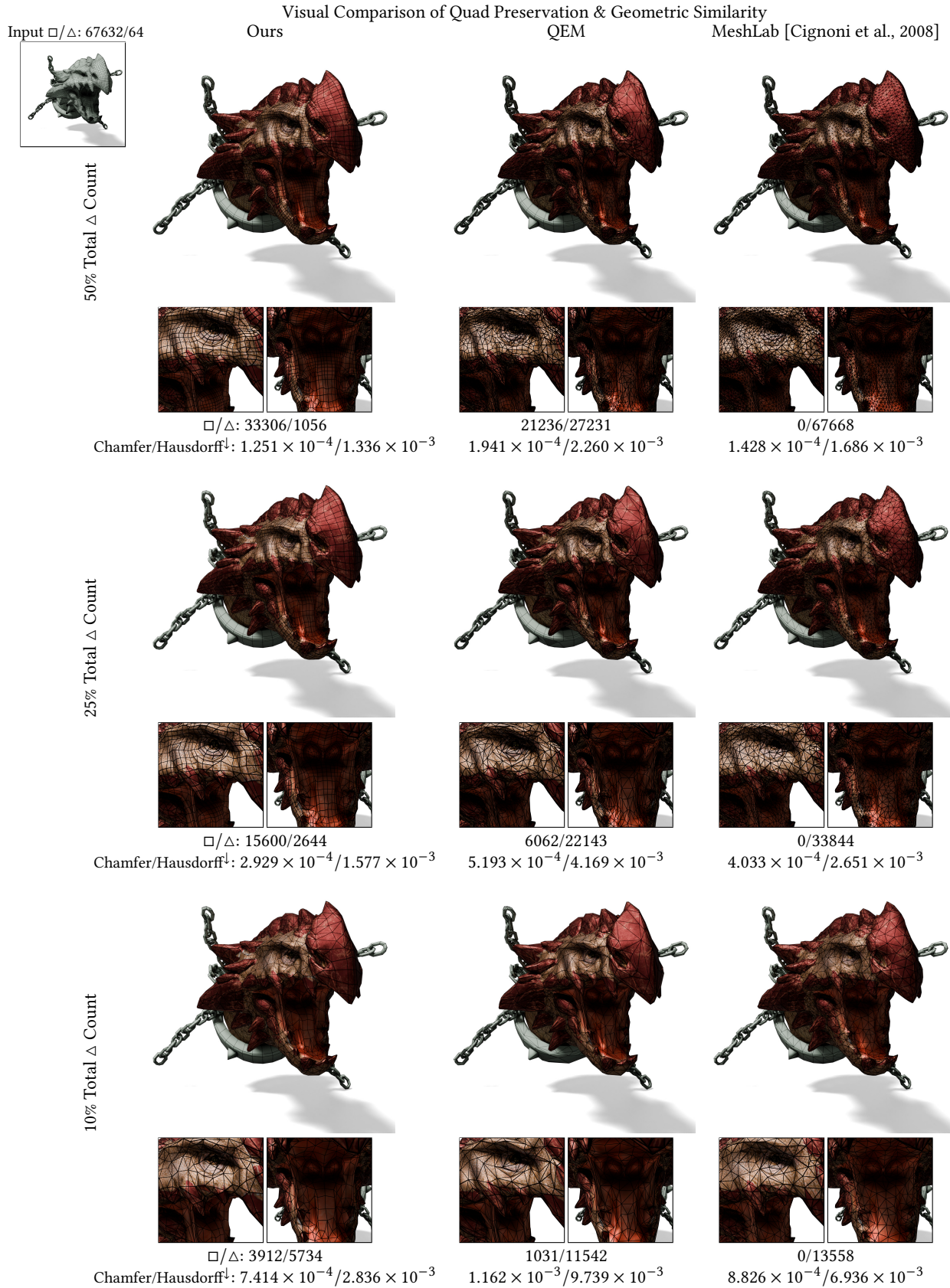


Fig. 7. Our approach compared to an implementation of [Hoppe, 1999] (labeled QEM) and [Cignoni et al., 2008] on a quad dominant mesh. Our approach is able to preserve more quads, while also having higher geometric similarity than other approaches. © ̄ricocilliers.

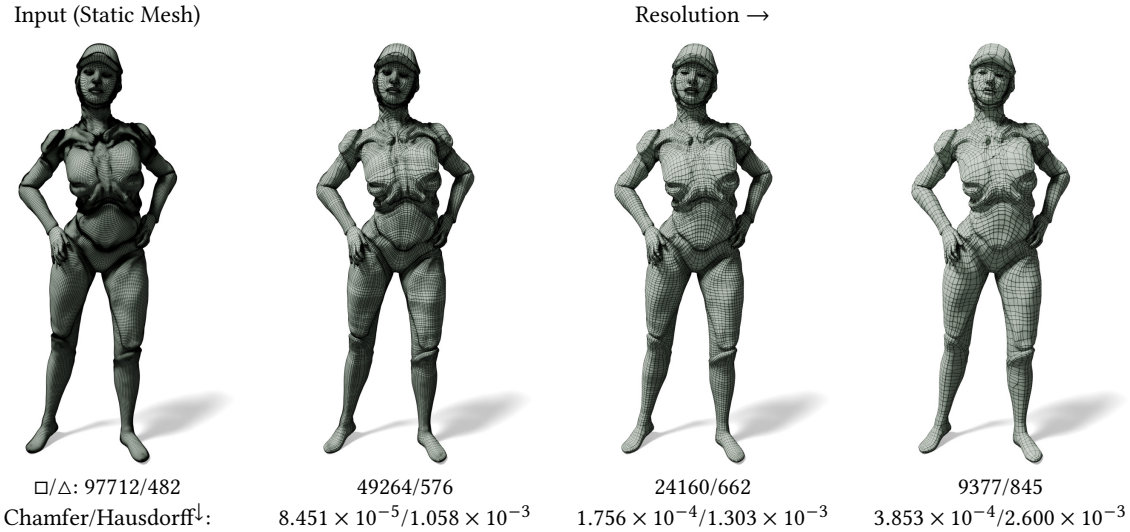


Fig. 8. Decimation of a hybrid quad mesh with many components at multiple resolutions. Our approach preserves most quads without sacrificing geometric quality using the edge collapse operator. Triangles are introduced between regions of varying quadric error, especially at lower resolutions. © Ploobert.

geometric similarity. Our approach has a smaller variance of geometric similarity while having a noticeable increase in the number of quads preserved. This demonstrates that our implementation is able to more consistently preserve quads from the input mesh, with no trade-off in geometric quality. [Cignoni et al., 2008] is omitted from this graph since it cannot preserve any quads.

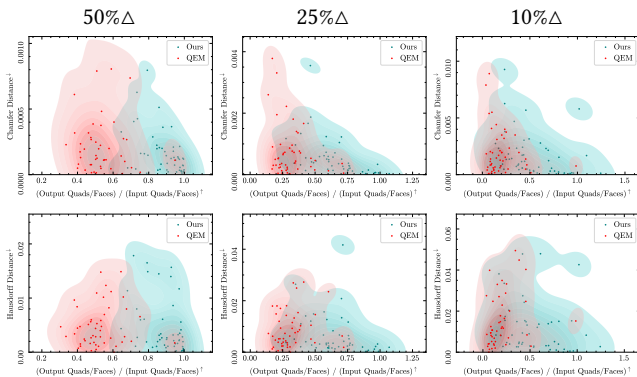


Fig. 9. Visualization of quad preservation against geometric quality for our approach and “QEM” for static meshes with one or more quads. Our approach preserves more quads and has higher geometric fidelity at all decimation levels. MeshLab [Cignoni et al., 2008] is not included since it cannot preserve any quads.

Qualitative Comparison. We visually compare our approach to QEM and [Cignoni et al., 2008] in Fig. 7 for a single static mesh with UVs and texture at multiple resolutions. The input is a quad-dominant character mesh, which contains 67632 quads and 64 triangles. At 50% of the input total triangle count ($2 \times \#quads + \#triangles$), our approach visually looks to be a quad-dominant mesh, and has

96% of its faces as quads. One example region where our approach preserves more quads is the nose where our approach retains the original quad structure from the input at 50% and 25% triangle ratios. In contrast, QEM and [Cignoni et al., 2008] destroy the quad topology of the nose. Meshlab preserves some of the input structure, but since it requires that the input be triangulated it is harder to tell. At 25% of the input triangle count, our approach is able to preserve most quads (86%), and introduces some triangles between regions of varying quadric error. QEM and [Cignoni et al., 2008], on the other hand at this point have removed most of the input topology, except around the collar. At 10% of the input total triangle count, our approach introduces a larger number of triangles, with 41% of all faces being quads. Our approaches introduces these triangle as pure quad preservation would sacrifice geometric quality. While there are still some quad elements in our approach, in QEM or [Cignoni et al., 2008] it is difficult to recognize any of the input topology.

We also show an example of only our approach at different resolutions on another hybrid quad mesh in Fig. 8, where we have increased ϵ_{abs} to 1×10^{-4} , leading to higher quad preservation. Our approach preserves the original quad topology at all levels of reduction, with visible quad structure at every step.

Animated Meshes. To compare our approach on animated meshes, we decimate each animated mesh to 50%, 25%, and 10% of the input mesh’s triangle count. We then compute the Chamfer and Hausdorff distance at the first 50 frames of the first animation for each mesh. Plots of frame number against geometric similarity for each model are shown in the Appendix, Fig. 19. We find that across the dataset, our approach outperforms QEM on both Hausdorff and Chamfer distances for most meshes. Specifically, we find that adapting [Hoppe, 1999] to preserve joint influences outperforms [Landreneau and Schaefer, 2009] on the majority of models for all frames, as shown in Tab. 2. In Tab. 2, we count the number of models where the average

is lower across the first 50 frames. We also show a visual comparison of animated mesh reduction in the Appendix, Fig. 20.

Skinned Mesh Reduction Geometric Stats

Metric	QEM	Ours
50% Δ		
#Lower Avg. Chamfer	1	18
#Lower Avg. Hausdorff	5	14
25% Δ		
#Lower Avg. Chamfer	3	16
#Lower Avg. Hausdorff	5	14
25% Δ		
#Lower Avg. Chamfer	1	18
#Lower Avg. Hausdorff	5	14

Table 2. Number of animated models where QEM (which implements [Lan-dreneau and Schaefer, 2009]) versus our approach has lower average geometric distance on the first 50 frames. Our approach, which uses [Hoppe, 1999] to preserve joint influence consistently outperforms the baseline. Full plots showing the Chamfer and Hausdorff distance per frame are shown in the Appendix, Fig. 19.

5.1 Symmetry Preservation

We show that our approach is able to identify and preserve key symmetries, by testing our approach on some example meshes with symmetries. This includes reflectional symmetry, as well as radial symmetry. Example outputs for reflectional symmetry are shown in Fig. 10, and for radial symmetry is shown in Fig. 11. Our approach is able to preserve a key axis of symmetry of the mech mesh, whereas QEM is unable to, especially along the head and lower part of the body. For radial symmetry preservation, the output has cleaner topology, for example the pipes extending from the central ring more closely resemble each other when including symmetry. We show 3 additional examples of symmetry in the Appendix, Fig. 18.

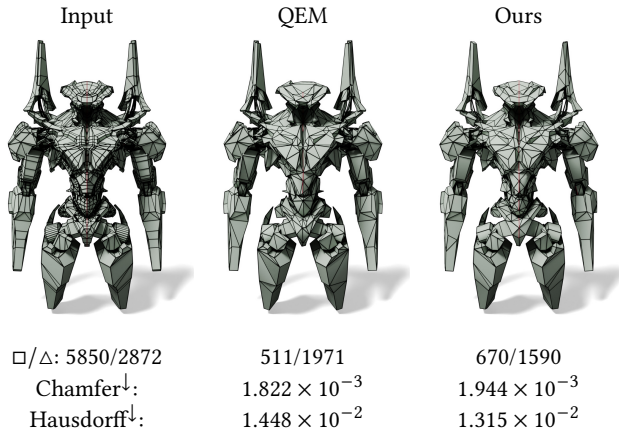


Fig. 10. As compared to normal QEM, our approach is able to preserve more topological symmetry, such as on the head of this mesh. The key axis of symmetry is shown in red for each mesh. © KhoMinh.

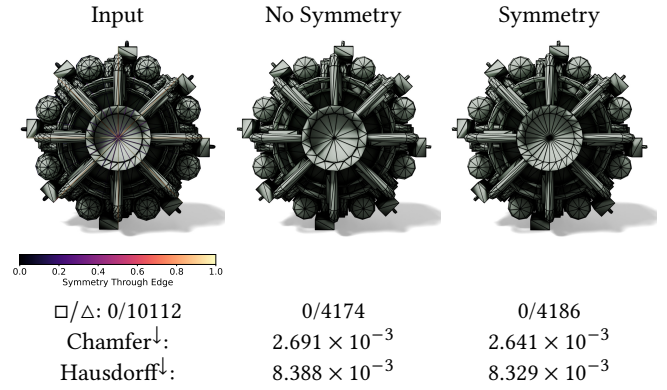


Fig. 11. Our approach identifies and preserves radial symmetry. Left: input mesh. Center: mesh with no symmetry preservation. Right: mesh with symmetry preservation. © Renafox.

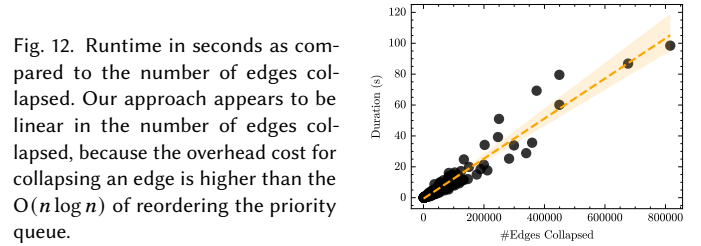


Fig. 12. Runtime in seconds as compared to the number of edges collapsed. Our approach appears to be linear in the number of edges collapsed, because the overhead cost for collapsing an edge is higher than the $O(n \log n)$ of reordering the priority queue.

5.2 Runtime

Quadric mesh reduction [Garland and Heckbert, 1997] has $O(n \log n)$ complexity with n being the number of edge collapses, but in practice has linear runtime, $O(n)$, as the cost of edge collapse dominates over reordering the priority queue. Our approach has $O(n \log n + k \log k)$, where k is the size of the second priority queue used to order equivalent edges. In practice $k \ll n$ and our approach has similar runtime to QEM. We visualize the runtime of our approach in Fig. 12, which is linear for the same reason that quadric mesh reduction is linear.

6 ABLATIONS

We ablate a number of parameters and design choices in our approach. Specifically, we compare our approach with and without priority based on recency of opposing quad edges, our new QEM formulation versus the original, selecting λ_{joint} , the importance of choosing ϵ_{abs} and ϵ_{rel} for comparing quadric errors, and why we use the dihedral angle to weigh the importance of each edge.

6.1 Recency

To demonstrate the importance of recency, we ablate our approach on a quad-dominant mesh decimated to 50% of the original triangle count, shown in Fig. 13. With recency, most quads are preserved, and the original edge flow is strongly preserved. Without recency, the edge flow is destroyed, and a large number of triangles are introduced. Most quads that remain are untouched from the original mesh. On the other hand, the geometric quality suffers slightly when including recency.

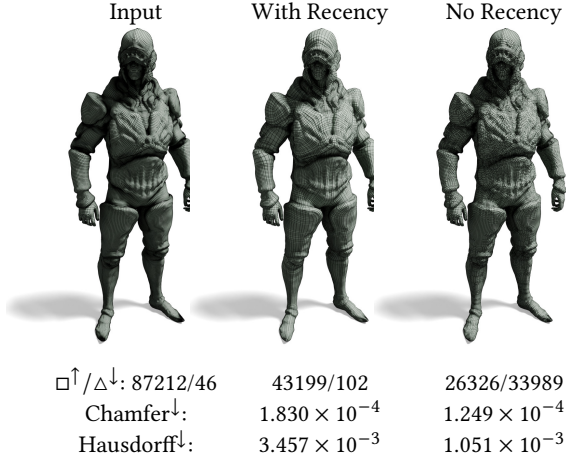


Fig. 13. We ablate our approach with and without recency on a complex mesh. When recency is disabled, the output mesh has is slightly more geometrically similar to the input mesh, but with significantly worse topology. Best Viewed Zoomed In. ©Ploobert.

6.2 New QEM Equation vs. Original

We ablate our new QEM formulation (Eq. 5) against the original QEM formulation on a single mesh in Fig. 14, both without memoryless simplification. There is geometric improvement using Eq. 5 as compared to the original QEM [Garland and Heckbert, 1997], and the topology of the result is closer to the original.

Comparison without Memoryless Simplification of QEM

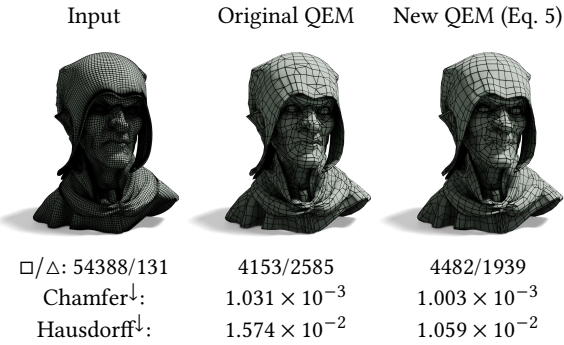


Fig. 14. Ablation of the new QEM formulation from Eq. 5 against the original QEM formulation from [Garland and Heckbert, 1997] without memoryless simplification. The new QEM formulation improves over the original when comparing geometric similarity. With our simplification approach, the new QEM leads to topology that more closely matches the input.

6.3 Edge Weighting (Eq. 2)

To demonstrate the importance of using the dihedral angle to weigh the importance of the per edge quadric, we test our approach by fixing w from Eq. 2 to $w = 0$ (no weights), $w = 1$ (uniform weights), and compare those to using dihedral angles to select a weight in Fig. 15. When including no weights, the position of quadrics in the

tangent space of coplanar faces are degenerate, leading to flipped, degenerate faces. When $w = 1$, sharp edges often become over-smoothed. With dihedral angles, sharp edges are kept sharp, as measured by the geometric similarity. On the left of Fig. 15, we visualize the distribution of dihedral angles of manifold edges in each mesh, not including angles below 0.5° . When using dihedral angles as weights, the output mesh’s distribution of angles more accurately matches the input mesh’s distribution.

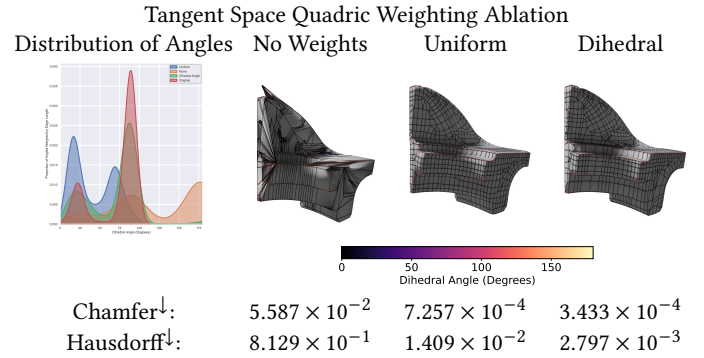


Fig. 15. We ablate our approach with different weights on tangent space quadric. The color of wireframe edges indicates dihedral angle, with redder being larger angle. The distribution shown does not include angles below 0.5° as they do not define geometric features and obscure the distribution. The dihedral-angle weighted distribution most closely matches the input mesh’s dihedral angle distribution.

6.4 Joint Distance λ_{joint}

To demonstrate the importance of weighing edges by joint distance, we compare our approach with $\lambda_{\text{joint}} = 0$, $\lambda_{\text{joint}} = 1$, $\lambda_{\text{joint}} = 10$. We focus primarily on the monster’s leg joint, which are bulbous regions with slightly higher density of edges than the rest of the leg. As λ_{joint} is increased, we see an increase in joint density in that region, at the cost of higher chamfer distance in the rest pose. When $\lambda_{\text{joint}} = 1$, there is a lower chamfer and Hausdorff distance across all frames as compared to $\lambda_{\text{joint}} = 0$ and $\lambda_{\text{joint}} = 10$. This makes it evident that some importance of quadrics along edges between vertices with highly variable joint influences help preserves animation quality.

6.5 Approximate Equality ϵ_{abs}

We also ablate our approach while varying ϵ_{abs} to demonstrate its impact on quad preservation and geometric quality.

We visualize the results of varying ϵ_{abs} in Fig. 17. Increasing ϵ_{abs} increases quad preservation, at the cost of lower geometric similarity, as can be seen when $\epsilon_{\text{abs}} = 1 \times 10^{-4}$, where the geometric distance increases by 1.5×10^{-4} from $\epsilon_{\text{abs}} = 1 \times 10^{-6}$ to 1×10^{-4} . Such a small change is likely unnoticeable to a viewer, so depending on the downstream application it may be worthwhile to trade this geometric difference to preserve more quads.

7 DISCUSSION

We develop modifications to the normal mesh reduction approach that are able to preserve the quad topology of input meshes at no

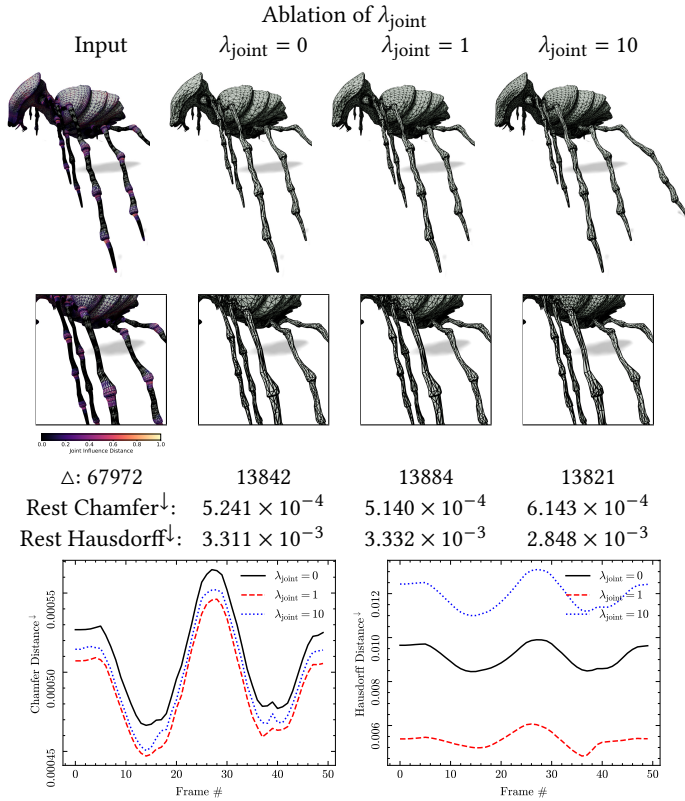


Fig. 16. Ablation of our approach with varying λ_{joint} . As λ_{joint} increases, the area around joints is more strongly preserved, at the cost of higher decimation in other areas. Despite the rest pose chamfer distance increasing, we see that at $\lambda_{\text{joint}} = 1$ there is an improvement to both the hausdorff and chamfer distance during animation, whereas when $\lambda_{\text{joint}} = 10$ there is too much preservation at joints, leading to lower geometric similarity during animation. ©️📧Rasmus.

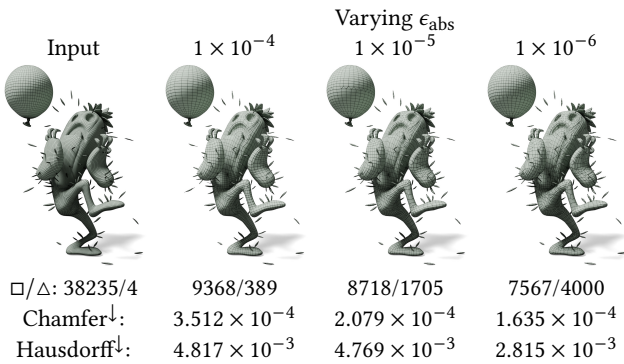


Fig. 17. We ablate the effect of varying ϵ_{abs} from Eq. 4. As ϵ_{abs} increases, there is stronger quad preservation, but a slight increase in the distance from the original mesh. ©️📧felipegall.

cost, and demonstrate how these modifications can be extended to preserve symmetry and joint influences. We have also performed

a thorough test demonstrating that [Hoppe, 1999] is suitable for joint preservation, producing more geometrically similar articulated outputs than [Landreneau and Schaefer, 2009] on most of our tested models.

For applications which require 100% quad preservation, our approach cannot provide such a guarantee, as it will usually introduce a small number of triangles between regions where quads have different quadric error. Furthermore, it is also possible to devise an adversarial quad mesh where opposing quad edges vary significantly, which may defeat our algorithm. In practice though, we observe most meshes contain regular quad elements and are amenable to our approach.

Our symmetry preservation technique is suitable primarily for smaller meshes, due to quadratic scaling with time complexity $O(|V||E|)$. For many of our test meshes though, this is acceptable, since the constant factor is low, and each edge's symmetry weight can be computed in parallel. Another problem with our approach to symmetry preservation is that it is less common for static meshes to contain extrinsic symmetry, but may contain intrinsic symmetry. Our approach to symmetry preservation is unable to identify intrinsic symmetries and thus cannot preserve them. Animated meshes, on the other hand, often contain a T-pose with extrinsic symmetries, which our approach is well-suited for. We leave exploration of intrinsic topological symmetry preservation to future work.

8 CONCLUSION

In summary, we develop a robust and simple approach that converts existing triangle quadric mesh reduction algorithms into quad-dominant mesh reduction algorithms, while maintaining the same or better geometric quality. Our approach is easily extended to handle symmetric decimation, joint preserving decimation, or generic edge painting to preserve certain regions more. Our primary insight in this work is that local operations ordered entirely by geometric error define too strict of an ordering, and by relaxing the ordering we are able to easily impose an ordering which preserves quads, and by extension topology. We hope this work is adopted by tooling so that mesh reduction on all platforms can better preserve input topology.

REFERENCES

- Å. Björck. 1994. Numerics of Gram-Schmidt orthogonalization. *Linear Algebra Appl.* 197-198 (1994), 297-316. [https://doi.org/10.1016/0024-3795\(94\)90493-6](https://doi.org/10.1016/0024-3795(94)90493-6)
- Blender Online Community. 2018. *Blender - a 3D modelling and rendering package*. Blender Foundation, Stichting Blender Foundation, Amsterdam. <http://www.blender.org>
- Agostino Bozzo, Daniele Panozzo, Enrico Puppo, Nico Pietroni, and Luigi Rocca. 2010. Adaptive Quad Mesh Simplification. In *Eurographics Italian Chapter Conference 2010*, Enrico Puppo, Andrea Brogni, and Leila De Floriani (Eds.). The Eurographics Association. <https://doi.org/10.2312/LocalChapterEvents/ItalChap/ItalianChapConf2010/095-102>
- Tyson Brochu, Essex Edwards, and Robert Bridson. 2012. Efficient geometrically exact continuous collision detection. *ACM Trans. Graph.* 31, 4, Article 96 (July 2012), 7 pages. <https://doi.org/10.1145/2185520.2185592>
- Gianmarco Cherchi, Marco Livesu, Riccardo Scateni, and Marco Attene. 2020. Fast and Robust Mesh Arrangements using Floating-point Arithmetic. *ACM Transactions on Graphics (SIGGRAPH Asia 2020)* 39, 6 (2020). <https://doi.org/10.1145/3414685.3417818>
- Paolo Cignoni, Marco Callieri, Massimiliano Corsini, Matteo Dellepiane, Fabio Ganovelli, and Guido Ranzuglia. 2008. MeshLab: an Open-Source Mesh Processing Tool. In *Eurographics Italian Chapter Conference*, Vittorio Scarano, Rosario De Chiara, and Ugo Erra (Eds.). The Eurographics Association. <https://doi.org/10.2312/LocalChapterEvents/ItalChap/ItalianChapConf2008/129-136>

- Joel Daniels, Cláudio T. Silva, Jason Shepherd, and Elaine Cohen. 2008. Quadrilateral mesh simplification. In *ACM SIGGRAPH Asia 2008 Papers* (Singapore) (*SIGGRAPH Asia '08*). Association for Computing Machinery, New York, NY, USA, Article 148, 9 pages. <https://doi.org/10.1145/1457515.1409101>
- Bruce Dawson. 2012. Comparing floating point numbers, 2012 edition. <https://randomascii.wordpress.com/2012/02/25/comparing-floating-point-numbers-2012-edition/>
- Christopher DeCoro and Szymon Rusinkiewicz. 2005. Pose-independent simplification of articulated meshes. In *Proceedings of the 2005 Symposium on Interactive 3D Graphics and Games* (Washington, District of Columbia) (*I3D '05*). Association for Computing Machinery, New York, NY, USA, 17–24. <https://doi.org/10.1145/1053427.1053430>
- Donya Labs AB. 2022. Simplygon 10. <https://www.simplygon.com/>
- Epic Games. 2022. Unreal Engine 5. <https://www.unrealengine.com/en-US/unreal-engine-5>
- Anton Fuhrmann and Dieter Schmalstieg. 1999. Coarse View-Dependent Levels of Detail for Hierarchical and Deformable Models. TR-186-2-99-20 Vienna University of Technology; ? ; Conference date: 31-12-1999 Through 31-12-1999.
- Michael Garland and Paul S. Heckbert. 1997. Surface Simplification Using Quadric Error Metrics. In *Proceedings of the 24th Annual Conference on Computer Graphics and Interactive Techniques* (*SIGGRAPH '97*). ACM Press/Addison-Wesley Publishing Co., USA, 209–216. <https://doi.org/10.1145/258734.258849>
- Michael Garland and Paul S. Heckbert. 1998. Simplifying surfaces with color and texture using quadric error metrics. In *Proceedings of the Conference on Visualization '98* (Research Triangle Park, North Carolina, USA) (*VIS '98*). IEEE Computer Society Press, Washington, DC, USA, 263–269.
- Christian Hafner, Mickaël Ly, and Chris Wojtan. 2024. Spin-It Faster: Quadrics Solve All Topology Optimization Problems That Depend Only On Mass Moments. *ACM Trans. Graph.* 43, 4, Article 78 (July 2024), 13 pages. <https://doi.org/10.1145/3658194>
- Hugues Hoppe. 1999. New quadric metric for simplifying meshes with appearance attributes. In *Proceedings of the Conference on Visualization '99: Celebrating Ten Years* (San Francisco, California, USA) (*VIS '99*). IEEE Computer Society Press, Washington, DC, USA, 59–66.
- Jocelyn Houle and Pierre Poulin. 2001. Simplification and Real-time Smooth Transitions of Articulated Meshes. In *Graphics Interface 2001*. 55–60.
- Yixin Hu, Teseo Schneider, Bolun Wang, Denis Zorin, and Daniele Panozzo. 2020. Fast Tetrahedral Meshing in the Wild. *ACM Trans. Graph.* 39, 4, Article 117 (July 2020), 18 pages. <https://doi.org/10.1145/3386569.3392385>
- Yixin Hu, Qingnan Zhou, Xifeng Gao, Alec Jacobson, Denis Zorin, and Daniele Panozzo. 2018. Tetrahedral Meshing in the Wild. *ACM Trans. Graph.* 37, 4, Article 60 (July 2018), 14 pages. <https://doi.org/10.1145/3197517.3201353>
- IEEE. 1985. *IEEE standard for binary floating-point arithmetic*. Institute of Electrical and Electronics Engineers, New York. Note: Standard 754–1985.
- Wenzel Jakob, Marco Tarini, Daniele Panozzo, and Olga Sorkine-Hornung. 2015. Instant Field-Aligned Meshes. *ACM Transactions on Graphics* (*Proceedings of SIGGRAPH ASIA*) 34, 6 (Nov. 2015). <https://doi.org/10.1145/2816795.2818078>
- W. Kahan. 1965. Pracniques: further remarks on reducing truncation errors. *Commun. ACM* 8, 1 (Jan. 1965), 40. <https://doi.org/10.1145/363707.363723>
- Eric Landreneau and Scott Schaefer. 2009. Simplification of Articulated Meshes. *Computer Graphics Forum* 28, 2 (2009), 347–353. <https://doi.org/10.1111/j.1467-8659.2009.01374.x> arXiv:<https://onlinelibrary.wiley.com/doi/pdf/10.1111/j.1467-8659.2009.01374.x>
- Bruno Lévy. 2019. Geogram. <http://alice.loria.fr/index.php/software/4-library/75-geogram.html>
- Hsueh-Ti Derek Liu, Xiaoting Zhang, and Cem Yuksel. 2024. Simplifying Triangle Meshes in the Wild. arXiv:2409.15458 [cs.GR] <https://arxiv.org/abs/2409.15458>
- Bruno Lévy. 2024. Exact predicates, exact constructions and combinatorics for mesh CSG. arXiv:2405.12949 [cs.CG] <https://arxiv.org/abs/2405.12949>
- Ashton Mason. 2020. Quad Mesh simplification in frostbite. https://ubm-tvvideo01.s3.amazonaws.com/o1/vault/gdc2020/presentations/Quad_Mesh_Simplification_Mason_Ashton.pdf
- Manfred M. Nerurkar. 2021. InstaLOD. <https://instalod.com>
- Nico Pietroni, Stefano Nuvoli, Thomas Alderighi, Paolo Cignoni, and Marco Tarini. 2021. Reliable feature-line driven quad-remeshing. *ACM Trans. Graph.* 40, 4, Article 155 (July 2021), 17 pages. <https://doi.org/10.1145/3450626.3459941>
- Bay Raitt and Greg Minter. 1998. Digital Sculpture Techniques (How to Apply the Principles of Traditional Sculpture to make Stunning 3D Characters). <https://web.archive.org/web/20160218133259/https://www.ualberta.ca/~cwant/blender/derived-surfaces.pdf#expand>
- Jonathan Richard Shewchuk. 1997. Adaptive precision floating-point arithmetic and fast robust geometric predicates. *Discrete & Computational Geometry* 18 (1997), 305–363.
- Ariel Shamir and Valerio Pascucci. 2001. Temporal and spatial level of details for dynamic meshes. In *Proceedings of the ACM Symposium on Virtual Reality Software and Technology* (Baniff, Alberta, Canada) (*VRST '01*). Association for Computing Machinery, New York, NY, USA, 77–84. <https://doi.org/10.1145/505008.505023>
- Sketchfab. 2022. The best 3D viewer on the web. <https://sketchfab.com/>
- Marco Tarini, Nico Pietroni, Paolo Cignoni, Daniele Panozzo, and Enrico Puppo. 2010. Practical quad mesh simplification. *Computer Graphics Forum* 29, 2 (2010), 407–418. <https://doi.org/10.1111/j.1467-8659.2009.01610.x> arXiv:<https://onlinelibrary.wiley.com/doi/pdf/10.1111/j.1467-8659.2009.01610.x>
- Marco Tarini, Enrico Puppo, Daniele Panozzo, Nico Pietroni, and Paolo Cignoni. 2011. Simple quad domains for field aligned mesh parametrization. *ACM Trans. Graph.* 30, 6 (Dec. 2011), 1–12. <https://doi.org/10.1145/2070781.2024176>
- Jean-Marc Thiery, Emilie Guy, and Tamy Boubekeur. 2013. Sphere-Meshes: Shape Approximation using Spherical Quadric Error Metrics. *ACM Transaction on Graphics* (*Proc. SIGGRAPH Asia 2013*) 32, 6 (2013), Art. No. 178.
- Jean-Marc Thiery, Emilie Guy, Tamy Boubekeur, and Elmar Eisemann. 2016. Animated Mesh Approximation With Sphere-Meshes. *ACM Trans. Graph.* 35, 3, Article 30 (May 2016), 13 pages. <https://doi.org/10.1145/2898350>
- Philip Trettner and Leif Kobbelt. 2020. Fast and Robust QEF Minimization using Probabilistic Quadrics. *Computer Graphics Forum* (2020). <https://doi.org/10.1111/cgf.13933>
- Philip Trettner, Julius Nehring-Wirxel, and Leif Kobbelt. 2022. EMBER: exact mesh booleans via efficient & robust local arrangements. *ACM Trans. Graph.* 41, 4, Article 39 (July 2022), 15 pages. <https://doi.org/10.1145/3528223.3530181>
- Bolun Wang, Zachary Ferguson, Xin Jiang, Marco Attene, Daniele Panozzo, and Teseo Schneider. 2022. Fast and Exact Root Parity for Continuous Collision Detection. *Computer Graphics Forum* (*Proceedings of Eurographics*) 41, 2 (2022), 9 pages.
- Bolun Wang, Teseo Schneider, Yixin Hu, Marco Attene, and Daniele Panozzo. 2020. Exact and Efficient Polyhedral Envelope Containment Check. *ACM Trans. Graph.* 39, 4 (July 2020).
- Siqi Wang, Chenxi Liu, Daniele Panozzo, Denis Zorin, and Alec Jacobson. 2023. Bézier Spline Simplification Using Locally Integrated Error Metrics. In *SIGGRAPH Asia 2023 Conference Papers* (Sydney, NSW, Australia) (*SA '23*). Association for Computing Machinery, New York, NY, USA, Article 27, 11 pages. <https://doi.org/10.1145/3610548.3618248>
- Tong Zhao, Laurent Busé, David Cohen-Steiner, Tamy Boubekeur, Jean-Marc Thiery, and Pierre Alliez. 2023. Variational Shape Reconstruction via Quadric Error Metrics. In *ACM SIGGRAPH 2023 Conference Proceedings* (Los Angeles, CA, USA) (*SIGGRAPH '23*). Association for Computing Machinery, New York, NY, USA, Article 45, 10 pages. <https://doi.org/10.1145/3588432.3591529>

A ADDITIONAL RESULTS

In the appendix we include the algorithm for computing per edge symmetry in Alg 2. Then, we include additional examples of symmetric preservation in Fig. 18. We also include a table of summary statistics for our whole dataset in Tab. 3, and complete results of reduction on each individual model in Tab. 4, Tab. 5, and Tab. 6. Furthermore, we show Chamfer and Hausdorff distances on all animated models for the first 50 frames of animation in Fig. 19. Finally, we show two visual comparisons of animated mesh reduction in Fig. 20.

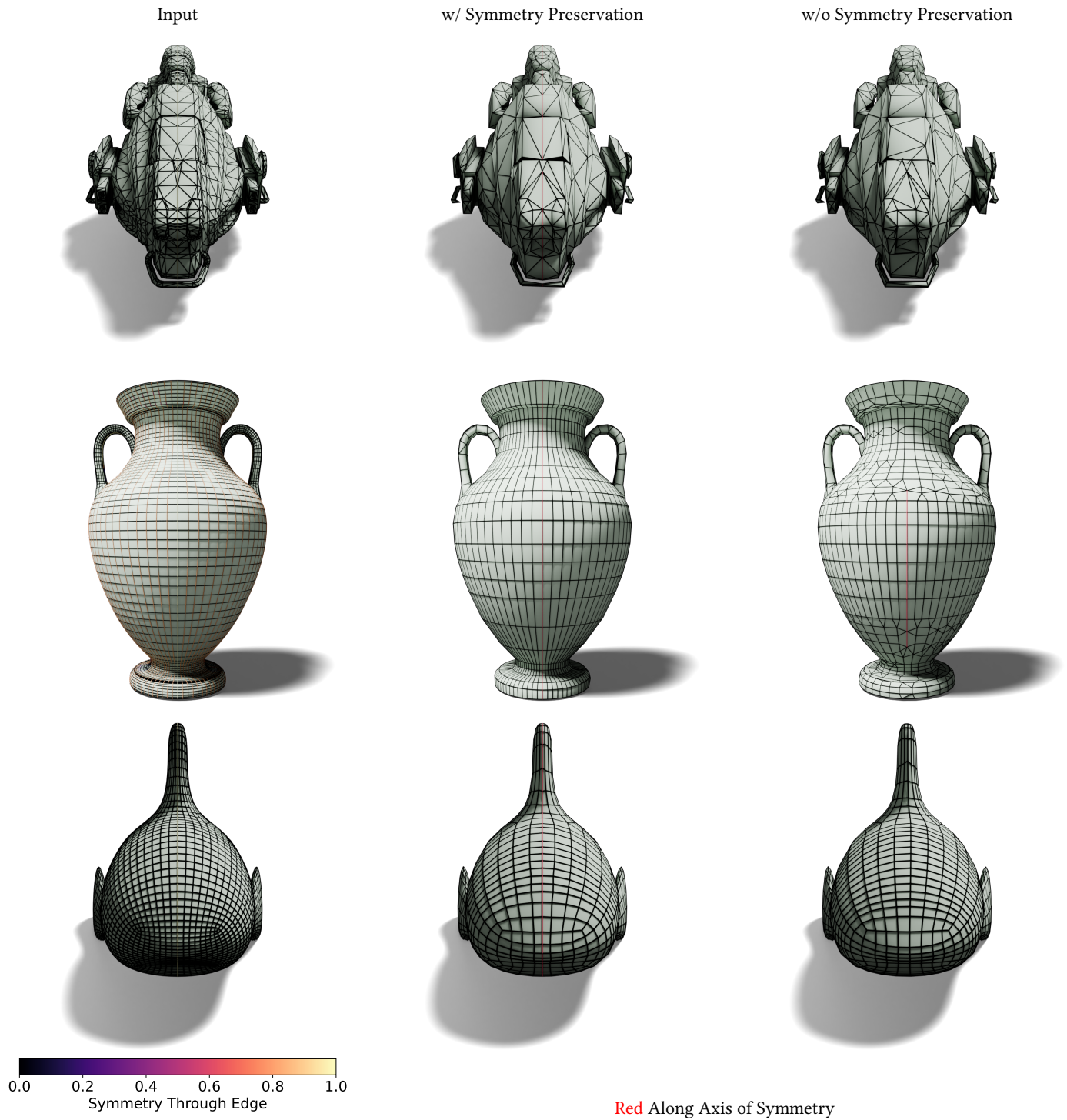


Fig. 18. We show additional examples of symmetry preservation on some example meshes. By increasing the weight of edges along planes of symmetry, our approach is able to preserve these edges on axes of symmetry in the output mesh topology. Note that for the bottom right mesh, even though it looks like the axis is preserved it is slightly offset from the center.

Name	Input $ F $	Input $ V $	Input \square	Input Δ	Source
Door Panel	64000	33599	0	64000	©Minneapolis Institute of Art
2B	1139322	920574	621539	517452	©MatheusEvan
Anak The Lizardman	165550	88385	0	165550	©Hawk
Angelica	78608	93049	64994	13574	©DarkNik
Angkor Wat	484200	293126	0	484200	©GSXNet
T-Rex Dinosaur Biting Attack	11938	6819	0	11938	©LasquetiSpice
Arches	14032	28540	14032	0	©Ayman Ibrahim
Armadillo	99976	49990	0	99976	The Stanford 3D Scanning Repository
Armored Charizard	4649	3273	12	4637	©projectmgame
Berserk Armor	19210	22470	0	19210	©Angy97
Bicycle	54995	102354	42464	10396	©wanderer
Blub Quadrangulated	7104	7317	7104	0	©Keenan Crane
Botchling	157549	164350	157140	409	©HD
Casio Keyboard	2804	3730	2649	0	©AleixoAlonso
Chimney Pipe	3404	4864	3404	0	©RubaQewar
Chitinous Knight	87258	89239	87212	46	©Ploobert
Cube	5756	7401	4236	1520	©Deslancer
Cuphead	35240	19820	0	35240	©AlmondFeather
Cyberpunk Bike	31916	37040	30488	1256	©daCruz
Dense Cube	1014	1176	1014	0	Handmade
Dragon With Pearl	999634	499803	0	999634	©Artec 3D
Dreadroamer	121482	81462	0	121482	©TooManyDemons
Dry Tree	149384	124158	0	149384	©Epic_Tree_Store
Egyptian Vase	7116	7557	7116	0	©Rijo
Etrian Odyssey 3 Monk	22821	14201	0	22821	©SChavafei
Fandisk	12946	6475	0	12946	Public Domain
Floral Pattern	104752	118792	104752	0	©RitorDP
French Halfbasket	35288	41255	35288	0	©leeeck
Globophobia	38239	41366	38235	4	©felipegall
Goblin Portrait	54519	57415	54388	131	©Vadik An
Greek Vase	12545	14464	12544	0	©Davide Specchi
Hercules Beetle	46892	140676	0	46892	©ArachnoBoy
His Name Is Violence	14416	18865	11778	2613	©Gleb Parshikov
Hover Bike	9327	7025	0	9327	©SPtis
Japanese House 2	233965	235330	233904	0	©neos_nelia
Japanese House 3	41462	42444	41298	132	©Karol
Japanese Shinto Shrine	6280	6638	5790	490	©Deerex
Kagiya Edo Tokyo	22819	18820	9855	12714	©t.c.
Lamborghini Countach	126970	152102	119160	5342	©SLevc16
Lantern	1360	1862	1328	32	©Blenderolokos
Lego Figure	3680	1938	0	3680	©Dirk.z
Lekythos	1075	1148	1075	0	©Global Digital Heritage and GDH-Afrika
Lethe	4782	8219	3986	789	©Klinepeter
Marble Track	32558	47029	26461	4566	©iin15101
Maze 45	37191	40663	37191	0	©Talaai-dev
Maze	37191	40663	37191	0	©Talaai-dev
Mech	8732	15771	5850	2872	©KhoaMinh
Medieval Knight	41654	31935	0	41654	©by_Rx
Melon Pallet	45016	45342	45016	0	©Duznot
Militech Robot	52349	29403	0	52349	©Ludovic Jouault
Timber Rattlesnake	240115	124297	0	240115	©DigitalLife3D
Walking Tokay Gecko Big Mama	7736	4491	0	7736	©DigitalLife3D
Southern Right Whale	36484	21547	0	36484	©DigitalLife3D
Southern White Rhino	64542	33743	0	64542	©DigitalLife3D
Atlantic Sturgeon	21856	11805	0	21856	©DigitalLife3D
Oni No Face Mask	219131	109564	0	219131	©warpnik
One Angry Dragon Boi	67696	74786	67632	64	©ricocilliers
Organic Armor	47270	48638	47270	0	©Ploobert
Pipe Wall	1545	1791	1543	2	©Aerial Knight
Prometheus	418183	400330	379559	38442	©Lapshin Sergey (in Cyrillic)
Radial	10112	7338	0	10112	©Renafox
Reap The Whirlwind	173179	109483	0	173179	©TooManyDemons
Roman Soldier	156714	148281	123893	32819	©Andy Woodhead
Rope Bridge	7256	7624	4444	2688	©lucq
Security Cyborg	29928	24106	0	29928	©fletcherkinnear
Shinto Watchtower	131367	134770	123508	6164	©Sin_nass
Shirakawago House	15965	21329	15867	96	©Lokomotto
Skyward Ddf Poco Ship	183177	143771	12207	170968	©Simon Jennings
Snowflake Orb	77418	38395	0	77418	©Craleigh
Space Fighter	34965	55060	34057	40	Free Standard Kerem Kavalci
Speeder Bike	11926	15152	11568	188	©TashaLime
Spiderthing Take 3	67972	37862	0	67972	©fuzzy4fox
Spiral Staircase	6358	7437	1400	3949	©Hoody468
Spot Quadrangulated	2928	3225	2928	0	Keenan Crane
Steel Guard -7Mb	14744	14559	0	14744	©Mehdi Shamsavan
Sword Queen	179602	119123	0	179602	©Mateusz Woliński
Tank	15306	21338	15063	203	©maxpsr
Teacup	5728	3093	5728	0	©miranda.j.rice
The Dark Wraith	119034	123271	80572	38462	©davidkong
The First Descendant	106120	95969	0	106120	©SCatholomew
Tuba Gunner Guardian Of Orchestria	66488	46167	0	66488	©Harr3D
Unstable Robot	208568	124703	0	208568	©kalsloos
Venice Mask	260391	173954	35201	225190	©DailyArt
Vera Posed	47790	66243	40269	7517	©JohnMesplay
War Tank	35126	68541	27758	7368	©larrynguyen
Yeahright	377344	377084	377344	0	©Keenan Crane

Table 3. Summary of our input dataset taken from meshes online. It consists of some full quad meshes, some full triangle meshes, and mix of hybrid meshes. Animated meshes are highlighted in orange.

Algorithm 2 Edge Symmetry Weights

```

1: Input: Vertices  $V$ , edges  $E$ , faces  $F$ , distance  $\delta$ 
2: Output: Per edge weights  $w \in [0, 1]^{|E|}$ 
3: for  $e = (e_0, e_1) \in E$  do
4:    $d = \frac{e_0 - e_1}{\|e_0 - e_1\|_2}$ 
5:   if  $e$  adjacent to  $f_0, f_1$  then                                ▶ Manifold Edges
6:      $n_{\perp} = \frac{n(f_0) + n(f_1)}{\|n(f_0) + n(f_1)\|_2} \times d$ 
7:   else if  $e$  adjacent to  $f_0$  then                                ▶ Boundary Edges
8:      $n_{\perp} = n(f_0) \times d$ 
9:   else                                                            ▶ Non-Manifold Edges
10:     $w[e] = 0$ 
11:    continue
12:   $\text{dists}_{\text{edge}} : \text{list of } \mathbb{R}^3$ 
13:  for  $v \in V$  do                                ▶ Local pos. of  $v$  in plane defined by edge
14:     $v_{\text{local}} = \text{local}(v, \text{origin} = e_0, x = n_{\perp}, y = d, z = n_{\perp} \times d)$ 
15:    if  $v_{\text{local}}[0] < \delta$  then                                ▶ dist to plane  $< \delta$ , match itself
16:       $\text{matched}(e) += 1$ 
17:      continue
18:    push  $v_{\text{local}}$  into  $\text{dists}_{\text{edge}}$ 
19:  Sort  $\text{dists}_{\text{edge}}$  by  $\text{abs}(v[0])$ 
20:  while not empty( $\text{dists}_{\text{edge}}$ ) do
21:     $[d, x, y] = \text{dists}_{\text{edge}}.\text{pop\_back}()$ 
22:    Select last  $k_0$  elements where  $|v[0] - d| < \delta$ 
23:    Sort last  $k_0$  elements by  $v[1]$  (local  $x$ )
24:    Select last  $k_1$  where  $|v[1] - x| < \delta$ 
25:    for  $v' = [d_n, x_n, y_n] \in \text{dists}_{\text{edge}}$  do
26:      ▶ Check if vertex is on opp. side of plane within  $\delta$ 
27:      if  $\|(d_n + d)^2 + (x_n - x)^2 + (y_n - y)^2\|_2 < \delta$  then
28:         $\text{matched}(e) += 2$ 
29:        Remove  $v'$  from  $\text{dists}_{\text{edge}}$ 
30:      break
31:    Sort last  $k_0$  by  $|v[0]|$                                 ▶ Reset last  $k_0$  to original state
32:   $w[e] = \frac{\text{matched}(e)}{|V|}$ 
return  $w$ 

```

50% Reduction			Ours			QEM			MeshLab		
Name	Out Δ	In \square	Out \square	Chamfer [↓]	Hausdorff [↓]	Out \square	Chamfer [↓]	Hausdorff [↓]	Out \square	Chamfer [↓]	Hausdorff [↓]
Door Panel	32007	0	0	1.008×10^{-4}	1.637×10^{-3}	0	2.049×10^{-4}	3.336×10^{-3}	0	1.610×10^{-4}	1.404×10^{-3}
2B	880826	621539	279096	3.421×10^{-5}	1.959×10^{-3}	173585	3.476×10^{-5}	2.119×10^{-3}	0	4.078×10^{-5}	8.862×10^{-4}
Angelic	71861	64994	26721	4.047×10^{-4}	1.783×10^{-2}	23367	4.007×10^{-4}	2.371×10^{-2}	0	2.501×10^{-4}	7.024×10^{-3}
Angkor Wat	242128	0	0	3.499×10^{-5}	4.247×10^{-4}	0	4.713×10^{-5}	2.190×10^{-3}	0	4.873×10^{-5}	8.047×10^{-4}
Arches	14032	14032	6860	2.043×10^{-5}	2.440×10^{-4}	3302	1.302×10^{-5}	4.698×10^{-3}	0	2.507×10^{-4}	1.074×10^{-3}
Armadillo	49994	0	0	1.321×10^{-4}	5.599×10^{-4}	0	1.949×10^{-4}	2.758×10^{-3}	0	1.242×10^{-4}	9.217×10^{-4}
Armored Charizard	2332	12	12	5.494×10^{-4}	1.959×10^{-2}	12	9.968×10^{-4}	8.160×10^{-3}	0	8.056×10^{-4}	1.222×10^{-2}
Bicycle	60824	41618	20601	5.517×10^{-5}	3.485×10^{-3}	25297	5.306×10^{-5}	2.016×10^{-3}	0	2.334×10^{-4}	5.542×10^{-3}
Blub Quadrangulated	7104	7104	3505	2.149×10^{-4}	2.264×10^{-3}	2866	2.672×10^{-4}	7.983×10^{-3}	0	1.726×10^{-4}	1.467×10^{-3}
Botchling	157349	157140	78206	7.155×10^{-5}	2.838×10^{-3}	55701	6.314×10^{-5}	2.838×10^{-3}	0	6.250×10^{-5}	8.536×10^{-4}
Casio Keyboard	3448	2649	1018	1.232×10^{-4}	1.397×10^{-2}	1206	7.605×10^{-5}	5.985×10^{-3}	0	4.232×10^{-4}	1.537×10^{-2}
Chimney Pipe	3429	3404	1633	2.128×10^{-5}	1.099×10^{-3}	1186	1.252×10^{-4}	5.281×10^{-3}	0	6.837×10^{-4}	1.201×10^{-2}
Chitinous Knight	87234	87212	43427	1.248×10^{-4}	1.031×10^{-3}	26437	1.301×10^{-4}	1.109×10^{-3}	0	1.265×10^{-4}	8.789×10^{-4}
Cube	4998	4236	1885	2.877×10^{-4}	8.978×10^{-4}	1205	2.351×10^{-4}	1.521×10^{-3}	0	1.078×10^{-3}	2.095×10^{-2}
Cyberpunk Bike	31513	30488	14602	3.656×10^{-4}	1.567×10^{-2}	11502	1.993×10^{-4}	8.200×10^{-3}	0	2.865×10^{-4}	3.407×10^{-3}
Dense Cube	1014	1014	390	2.122×10^{-10}	1.517×10^{-9}	386	3.642×10^{-17}	4.095×10^{-14}	0	9.377×10^{-5}	5.942×10^{-4}
Dragon With Pearl	500166	0	0	5.063×10^{-5}	2.129×10^{-4}	0	8.399×10^{-5}	9.741×10^{-4}	0	5.367×10^{-5}	5.401×10^{-4}
Dreadroamer	63676	0	0	5.936×10^{-5}	2.732×10^{-3}	0	1.307×10^{-4}	1.907×10^{-3}	0	1.380×10^{-4}	2.111×10^{-3}
Dry Tree	74701	0	0	2.814×10^{-4}	5.847×10^{-2}	0	7.536×10^{-4}	6.081×10^{-2}	0	1.951×10^{-4}	4.280×10^{-3}
Egyptian Vase	7116	7116	3368	1.447×10^{-4}	8.356×10^{-4}	2081	3.179×10^{-4}	3.389×10^{-3}	0	2.787×10^{-4}	2.162×10^{-3}
Fandisk	6472	0	0	5.102×10^{-5}	4.440×10^{-4}	0	1.625×10^{-3}	1.225×10^{-2}	0	2.058×10^{-5}	5.116×10^{-5}
Floral Pattern	104752	104752	52027	1.183×10^{-5}	2.344×10^{-4}	41679	5.210×10^{-8}	1.088×10^{-3}	0	2.128×10^{-5}	4.580×10^{-4}
French Halfbasket	35289	35288	17588	2.596×10^{-5}	3.358×10^{-4}	11631	1.524×10^{-5}	2.781×10^{-4}	0	1.983×10^{-5}	2.450×10^{-4}
Globophobia	38245	38235	18797	1.259×10^{-4}	3.233×10^{-3}	13057	1.456×10^{-4}	1.355×10^{-3}	0	1.123×10^{-4}	3.771×10^{-3}
Goblin Portrait	54458	54388	26332	2.100×10^{-4}	3.183×10^{-3}	18645	2.477×10^{-4}	2.856×10^{-3}	0	2.589×10^{-4}	3.083×10^{-3}
Greek Vase	12575	12544	6155	1.356×10^{-4}	1.617×10^{-3}	5182	7.366×10^{-4}	2.423×10^{-2}	0	2.673×10^{-4}	4.101×10^{-3}
His Name Is Violence	13137	11778	5485	3.610×10^{-4}	6.078×10^{-3}	4097	3.753×10^{-4}	5.856×10^{-3}	0	2.906×10^{-4}	6.026×10^{-3}
Hover Bike	4662	0	0	8.741×10^{-4}	6.274×10^{-3}	0	1.128×10^{-5}	7.728×10^{-3}	0	1.371×10^{-3}	8.046×10^{-3}
Japanese House 2	234803	233904	116504	1.558×10^{-5}	2.067×10^{-4}	85340	1.331×10^{-6}	1.711×10^{-3}	0	5.733×10^{-5}	9.506×10^{-6}
Japanese House 3	41412	41298	20374	1.167×10^{-4}	2.141×10^{-3}	13169	1.736×10^{-4}	4.738×10^{-3}	0	1.547×10^{-4}	3.923×10^{-3}
Japanese Shinto Shrine	6104	5790	2706	4.005×10^{-5}	2.312×10^{-3}	2193	4.513×10^{-5}	2.600×10^{-3}	0	6.975×10^{-5}	2.813×10^{-3}
Kagiya Edo Tokyo	17192	9855	3911	1.596×10^{-4}	6.086×10^{-3}	3982	2.743×10^{-4}	1.020×10^{-2}	0	2.338×10^{-4}	1.951×10^{-2}
Lamorghini Countach	130216	119160	45823	5.152×10^{-5}	1.136×10^{-2}	47205	4.759×10^{-5}	1.479×10^{-2}	0	1.380×10^{-4}	2.885×10^{-3}
Lantern	1344	1328	558	4.366×10^{-5}	1.099×10^{-3}	402	4.931×10^{-5}	4.443×10^{-3}	0	6.126×10^{-5}	1.923×10^{-3}
Lego Figure	1839	0	0	2.085×10^{-4}	3.038×10^{-3}	0	2.132×10^{-4}	2.013×10^{-3}	0	1.021×10^{-4}	2.683×10^{-3}
Lekythos	1075	1075	455	6.272×10^{-4}	7.990×10^{-3}	318	1.283×10^{-5}	8.395×10^{-3}	0	7.744×10^{-4}	5.444×10^{-3}
Lethe	4395	3986	1696	1.617×10^{-4}	5.983×10^{-3}	1389	2.232×10^{-4}	3.999×10^{-3}	0	3.113×10^{-4}	4.510×10^{-3}
Marble Track	32376	26461	11444	1.478×10^{-4}	1.487×10^{-2}	11578	1.424×10^{-4}	1.487×10^{-2}	0	4.012×10^{-4}	2.699×10^{-2}
Maze 45	37207	37191	18441	2.313×10^{-5}	4.135×10^{-3}	13217	1.104×10^{-4}	1.016×10^{-2}	0	5.387×10^{-4}	7.673×10^{-4}
Maze	37200	37191	18432	3.098×10^{-5}	5.571×10^{-3}	13227	1.129×10^{-4}	6.960×10^{-3}	0	5.614×10^{-8}	1.347×10^{-3}
Mech	7312	5850	2208	3.259×10^{-4}	4.357×10^{-3}	1965	4.821×10^{-4}	4.754×10^{-3}	0	5.377×10^{-4}	7.779×10^{-3}
Melon Pallet	45047	45016	20636	2.242×10^{-4}	1.074×10^{-3}	15452	1.970×10^{-4}	1.082×10^{-3}	0	1.230×10^{-4}	3.246×10^{-3}
Militech Robot	26181	0	0	2.175×10^{-4}	4.337×10^{-3}	0	2.608×10^{-4}	3.573×10^{-3}	0	2.445×10^{-4}	6.062×10^{-3}
One Angry Dragon Boi	67673	67632	32971	1.104×10^{-4}	1.572×10^{-3}	21239	1.946×10^{-4}	2.421×10^{-3}	0	1.430×10^{-4}	1.686×10^{-3}
Oni No Face Mask	109580	0	0	4.541×10^{-5}	2.390×10^{-3}	0	8.324×10^{-5}	2.391×10^{-3}	0	3.087×10^{-5}	2.370×10^{-3}
Organic Armor	47270	47270	23584	1.183×10^{-4}	6.573×10^{-4}	13875	7.988×10^{-5}	7.338×10^{-4}	0	8.295×10^{-5}	5.220×10^{-4}
Pipe Wall	1544	1543	682	7.953×10^{-4}	1.650×10^{-2}	446	6.107×10^{-4}	9.632×10^{-3}	0	2.914×10^{-4}	6.592×10^{-3}
Prometheus	399528	379559	179616	3.606×10^{-5}	2.362×10^{-3}	125942	1.927×10^{-5}	1.805×10^{-3}	0	3.153×10^{-5}	6.506×10^{-4}
Radial	5056	0	0	6.918×10^{-4}	6.173×10^{-3}	0	7.935×10^{-4}	1.185×10^{-2}	0	1.440×10^{-3}	8.309×10^{-3}
Roman Soldier	140324	123893	60017	7.265×10^{-5}	1.083×10^{-3}	38795	7.583×10^{-5}	1.617×10^{-3}	0	9.637×10^{-5}	1.624×10^{-3}
Rope Bridge	6160	4444	2422	2.333×10^{-4}	1.093×10^{-3}	2563	1.100×10^{-4}	1.718×10^{-3}	0	7.980×10^{-5}	6.571×10^{-3}
Shinto Watchtower	132166	123508	60136	6.878×10^{-5}	1.941×10^{-3}	54203	1.005×10^{-4}	2.867×10^{-3}	0	6.460×10^{-5}	4.144×10^{-3}
Shirakawago House	15919	15867	7327	5.123×10^{-4}	1.447×10^{-2}	5627	7.896×10^{-4}	1.093×10^{-2}	0	2.747×10^{-4}	1.622×10^{-2}
Skyward Ddf Poco Ship	97819	12207	4884	9.907×10^{-6}	1.903×10^{-3}	4079	7.822×10^{-6}	1.869×10^{-3}	0	2.287×10^{-5}	9.664×10^{-4}
Snowflake Orb	38708	0	0	1.379×10^{-4}	8.018×10^{-4}	0	1.628×10^{-4}	1.070×10^{-3}	0	8.414×10^{-5}	1.248×10^{-3}
Space Fighter	36326	34057	16311	3.317×10^{-5}	1.170×10^{-2}	16499	1.799×10^{-5}	6.564×10^{-3}	0	9.965×10^{-5}	1.242×10^{-2}
Speeder Bike	12133	11568	5629	1.782×10^{-4}	8.615×10^{-3}	3999	2.829×10^{-4}	5.627×10^{-3}	0	2.177×10^{-4}	6.727×10^{-3}
Spiral Staircase	7270	1400	680	1.978×10^{-4}	1.838×10^{-1}	3329	1.672×10^{-4}	4.361×10^{-3}	0	1.666×10^{-4}	6.631×10^{-3}
Spot Quadrangulated	2930	2928	1243	4.262×10^{-4}	2.733×10^{-3}	1087	8.052×10^{-4}	1.119×10^{-2}	0	6.648×10^{-4}	4.017×10^{-3}
Steel Guard -7Mb	7372	0	0	4.162×10^{-5}	2.044×10^{-4}	0	5.118×10^{-5}	8.723×10^{-4}	0	1.225×10^{-4}	3.812×10^{-3}
Tank	15229	15063	7108	1.754×10^{-4}	1.313×10^{-3}	4938	3.182×10^{-4}	5.119×10^{-3}	0	3.228×10^{-4}	5.113×10^{-3}
Teacup	5728	5728	2673	2.003×10^{-4}	2.658×10^{-3}	1968	3.863×10^{-4}	3.057×10^{-3}	0	3.819×10^{-4}	7.812×10^{-3}
The Dark Wraith	99833	80572	36976	7.980×10^{-5}	3.393×10^{-3}	25796	1.168×10^{-4}	4.388×10^{-3}	0	1.126×10^{-4}	3.744×10^{-3}
Venice Mask	147837	35201	16699	1.310×10^{-4}	2.131×10^{-3}	6497	2.284×10^{-4}	2.910×10^{-3}	0	1.670×10^{-4}	1.308×10^{-3}
Vera Posed	44056	40269	18506	2.058×10^{-4}	3.133×10^{-3}	13161	2.675×10^{-4}	2.661×10^{-3}	0	3.017×10^{-4}	3.115×10^{-3}
War Tank	31460	27758	13108	8.595×10^{-5}	2.656×10^{-3}	9875	1.134×10^{-4}	1.233×10^{-2}	0	1.642×10^{-3}	1.739×10^{-2}
Yeahright	377346	377344	188536	3.682×10^{-5}	4.155×10^{-4}	128378	1.385×10				

Name	25% Reduction			Ours			QEM			MeshLab		
	Out Δ	In \square	Out \square	Chamfer ¹	Hausdorff ¹	Out \square	Chamfer ¹	Hausdorff ¹	Out \square	Chamfer ¹	Hausdorff ¹	
Door Panel	16039	0	0	1.946×10^{-4}	1.989×10^{-3}	0	3.378×10^{-4}	7.587×10^{-3}	0	2.807×10^{-4}	1.652×10^{-3}	
2B	440761	621539	151889	6.818×10^{-5}	2.224×10^{-3}	52166	1.277×10^{-4}	2.380×10^{-3}	0	1.073×10^{-4}	1.787×10^{-3}	
Angelica	36211	64994	8112	9.674×10^{-4}	2.639×10^{-2}	7827	1.404×10^{-3}	2.491×10^{-2}	0	8.762×10^{-4}	1.341×10^{-2}	
Angkor Wat	121246	0	0	7.128×10^{-5}	9.543×10^{-4}	0	1.074×10^{-4}	3.108×10^{-3}	0	1.027×10^{-4}	1.540×10^{-3}	
Arches	7016	14032	3254	9.316×10^{-5}	2.009×10^{-3}	862	2.600×10^{-3}	7.268×10^{-3}	0	3.432×10^{-4}	1.028×10^{-2}	
Armadillo	25038	0	0	2.659×10^{-4}	9.818×10^{-4}	0	4.744×10^{-4}	4.352×10^{-3}	0	2.657×10^{-4}	1.465×10^{-3}	
Armored Charizard	1169	12	12	1.962×10^{-3}	2.836×10^{-2}	12	2.694×10^{-3}	1.968×10^{-2}	0	3.202×10^{-3}	4.216×10^{-2}	
Bicycle	30465	41618	7937	1.382×10^{-4}	3.485×10^{-3}	9704	1.548×10^{-4}	3.682×10^{-3}	0	8.595×10^{-4}	7.065×10^{-3}	
Blub Quadrangulated	3558	7104	1441	3.576×10^{-4}	2.134×10^{-3}	869	7.649×10^{-4}	1.152×10^{-2}	0	4.538×10^{-4}	2.874×10^{-3}	
Botchling	78739	157140	34635	1.170×10^{-4}	2.838×10^{-3}	17895	1.840×10^{-4}	2.837×10^{-3}	0	1.541×10^{-4}	2.521×10^{-3}	
Casio Keyboard	1732	2649	439	5.059×10^{-4}	1.338×10^{-2}	623	4.607×10^{-4}	1.461×10^{-2}	0	8.921×10^{-4}	2.516×10^{-2}	
Chimney Pipe	1702	3404	733	3.713×10^{-4}	6.450×10^{-3}	455	3.810×10^{-4}	7.586×10^{-3}	0	1.509×10^{-3}	1.785×10^{-2}	
Chitinous Knight	43657	87212	18870	1.983×10^{-4}	1.159×10^{-3}	6740	3.032×10^{-4}	1.932×10^{-3}	0	2.578×10^{-4}	1.470×10^{-3}	
Cube	2512	4236	815	7.099×10^{-4}	1.306×10^{-3}	333	3.310×10^{-3}	6.898×10^{-2}	0	8.076×10^{-3}	8.500×10^{-2}	
Cyberpunk Bike	15841	30488	5535	6.163×10^{-4}	1.567×10^{-2}	4950	5.319×10^{-4}	1.047×10^{-2}	0	5.843×10^{-4}	5.152×10^{-3}	
Dense Cube	506	1014	211	2.311×10^{-10}	1.517×10^{-9}	120	7.735×10^{-17}	5.674×10^{-14}	0	1.664×10^{-4}	1.018×10^{-2}	
Dragon With Pearl	251698	0	0	1.075×10^{-4}	3.907×10^{-4}	0	1.921×10^{-4}	1.784×10^{-3}	0	1.162×10^{-4}	9.499×10^{-4}	
Dreadroamer	33380	0	0	2.487×10^{-4}	3.165×10^{-3}	0	4.761×10^{-4}	4.110×10^{-3}	0	4.775×10^{-4}	5.095×10^{-3}	
Dry Tree	37434	0	0	6.452×10^{-4}	5.841×10^{-2}	0	1.976×10^{-3}	9.498×10^{-2}	0	4.283×10^{-4}	4.755×10^{-3}	
Egyptian Vase	3566	7116	1201	4.449×10^{-4}	1.729×10^{-3}	541	9.039×10^{-4}	6.196×10^{-3}	0	9.441×10^{-4}	4.269×10^{-3}	
Fandisk	3236	0	0	9.921×10^{-5}	9.996×10^{-4}	0	2.523×10^{-3}	1.527×10^{-2}	0	9.716×10^{-6}	2.283×10^{-4}	
Floral Pattern	52380	104752	24658	3.309×10^{-5}	2.764×10^{-4}	10830	1.360×10^{-5}	2.429×10^{-3}	0	5.533×10^{-5}	3.001×10^{-3}	
French Halfbasket	17757	35288	7518	3.792×10^{-5}	2.863×10^{-4}	3151	4.361×10^{-5}	5.695×10^{-4}	0	6.204×10^{-5}	4.846×10^{-4}	
Globophobia	19155	38235	7163	1.756×10^{-4}	1.726×10^{-3}	3804	3.640×10^{-4}	3.330×10^{-3}	0	2.990×10^{-4}	7.217×10^{-3}	
Goblin Portrait	27331	54388	6910	3.722×10^{-4}	5.069×10^{-3}	5633	6.509×10^{-4}	3.900×10^{-3}	0	6.035×10^{-4}	3.614×10^{-3}	
Greek Vase	6309	12544	2369	4.882×10^{-4}	1.629×10^{-3}	1847	1.664×10^{-3}	2.724×10^{-2}	0	7.140×10^{-4}	8.103×10^{-3}	
His Name Is Violence	6637	11778	2092	9.448×10^{-4}	6.665×10^{-3}	1416	9.599×10^{-4}	9.267×10^{-3}	0	1.538×10^{-3}	2.599×10^{-2}	
Hover Bike	2331	0	0	2.584×10^{-3}	1.572×10^{-2}	0	2.633×10^{-3}	1.112×10^{-2}	0	3.395×10^{-3}	1.488×10^{-2}	
Japanese House 2	117401	233904	56987	5.703×10^{-5}	1.179×10^{-3}	28476	1.834×10^{-5}	2.066×10^{-3}	0	8.944×10^{-6}	1.048×10^{-4}	
Japanese House 3	20708	41298	5773	3.187×10^{-4}	2.111×10^{-3}	4021	3.283×10^{-4}	5.221×10^{-3}	0	3.717×10^{-4}	4.071×10^{-3}	
Japanese Shinto Shrine	3025	5790	1200	2.715×10^{-4}	4.168×10^{-2}	957	2.606×10^{-4}	5.111×10^{-3}	0	3.924×10^{-4}	1.574×10^{-2}	
Kagiyu Edo Tokyo	8611	9855	1764	5.702×10^{-4}	8.303×10^{-3}	1235	7.073×10^{-4}	1.027×10^{-2}	0	1.069×10^{-3}	2.821×10^{-2}	
Lamborghini Countach	65761	119160	15461	1.345×10^{-4}	1.409×10^{-2}	14162	1.393×10^{-4}	1.429×10^{-2}	0	3.950×10^{-4}	1.266×10^{-2}	
Lantern	676	1328	246	1.237×10^{-3}	2.920×10^{-3}	179	1.825×10^{-4}	7.984×10^{-3}	0	4.266×10^{-4}	5.975×10^{-3}	
Lego Figure	930	0	0	8.633×10^{-4}	8.914×10^{-3}	0	7.354×10^{-4}	6.224×10^{-3}	0	4.914×10^{-4}	1.477×10^{-2}	
Lekythos	541	1075	172	1.871×10^{-3}	1.208×10^{-2}	80	3.780×10^{-3}	1.792×10^{-2}	0	3.734×10^{-3}	1.204×10^{-2}	
Lethe	2205	3986	597	1.669×10^{-3}	1.351×10^{-1}	541	7.650×10^{-4}	8.717×10^{-3}	0	1.302×10^{-3}	1.467×10^{-2}	
Marble Track	16465	26461	4146	3.885×10^{-4}	1.487×10^{-2}	2408	3.099×10^{-4}	1.487×10^{-2}	0	6.366×10^{-4}	2.690×10^{-2}	
Maze 45	18606	37191	8088	2.121×10^{-4}	3.500×10^{-3}	3418	2.222×10^{-4}	1.200×10^{-2}	0	2.143×10^{-6}	3.366×10^{-3}	
Maze	18606	37191	8039	2.947×10^{-4}	5.200×10^{-3}	3523	2.447×10^{-4}	1.701×10^{-2}	0	2.605×10^{-6}	4.629×10^{-3}	
Mech	3706	5850	767	1.338×10^{-3}	1.101×10^{-2}	745	1.361×10^{-3}	1.539×10^{-2}	0	2.150×10^{-3}	1.197×10^{-2}	
Melon Pallet	22838	45016	7331	4.165×10^{-4}	2.776×10^{-3}	4071	5.394×10^{-4}	5.196×10^{-3}	0	2.956×10^{-4}	4.788×10^{-3}	
Militech Robot	13145	0	0	7.468×10^{-4}	6.058×10^{-3}	0	8.301×10^{-4}	7.448×10^{-3}	0	6.931×10^{-4}	6.965×10^{-3}	
One Angry Dragon Boi	33859	67632	14669	2.825×10^{-4}	2.752×10^{-3}	6068	5.199×10^{-4}	3.868×10^{-3}	0	4.019×10^{-4}	2.651×10^{-3}	
Oni No Face Mask	54844	0	0	1.014×10^{-4}	2.419×10^{-3}	0	2.212×10^{-4}	2.495×10^{-3}	0	8.108×10^{-3}	2.421×10^{-3}	
Organic Armor	23646	47270	11265	1.510×10^{-4}	7.198×10^{-4}	3469	1.847×10^{-4}	1.272×10^{-3}	0	1.776×10^{-4}	1.013×10^{-3}	
Pipe Wall	774	1543	245	3.548×10^{-3}	1.278×10^{-1}	135	1.951×10^{-3}	1.797×10^{-2}	0	1.812×10^{-3}	1.278×10^{-1}	
Prometheus	200452	379559	80874	6.088×10^{-5}	2.362×10^{-3}	41858	5.792×10^{-5}	1.899×10^{-3}	0	8.706×10^{-5}	1.339×10^{-3}	
Radial	2528	0	0	2.914×10^{-3}	1.421×10^{-2}	0	2.443×10^{-3}	2.055×10^{-2}	0	7.336×10^{-3}	2.997×10^{-2}	
Roman Soldier	70260	123893	26162	1.454×10^{-4}	1.083×10^{-3}	13148	2.407×10^{-4}	3.640×10^{-3}	0	2.507×10^{-4}	1.940×10^{-3}	
Rope Bridge	3080	4444	912	1.045×10^{-3}	6.704×10^{-3}	1061	3.612×10^{-4}	6.306×10^{-3}	0	1.654×10^{-4}	6.567×10^{-3}	
Shinto Watchtower	66193	123508	22678	4.236×10^{-4}	2.376×10^{-3}	17016	4.396×10^{-4}	3.724×10^{-3}	0	1.042×10^{-3}	7.490×10^{-3}	
Shirakawago House	7997	15867	3288	1.228×10^{-3}	2.083×10^{-2}	2068	1.806×10^{-3}	2.694×10^{-2}	0	1.015×10^{-3}	2.089×10^{-2}	
Skyward Ddf Poco Ship	53668	12207	3573	3.090×10^{-5}	1.902×10^{-3}	2252	4.774×10^{-5}	1.893×10^{-3}	0	8.694×10^{-5}	3.181×10^{-3}	
Snowflake Orb	19360	0	0	4.783×10^{-4}	3.925×10^{-3}	0	6.225×10^{-4}	4.489×10^{-3}	0	3.863×10^{-4}	4.554×10^{-3}	
Space Fighter	18179	34057	7087	1.417×10^{-4}	1.170×10^{-2}	7273	1.261×10^{-4}	2.351×10^{-2}	0	3.248×10^{-4}	1.242×10^{-2}	
Speeder Bike	6117	11568	2177	5.052×10^{-4}	1.269×10^{-2}	1290	7.277×10^{-4}	7.305×10^{-3}	0	7.627×10^{-4}	1.069×10^{-2}	
Spiral Staircase	3666	1400	431	3.344×10^{-4}	3.181×10^{-3}	1175	3.311×10^{-4}	5.227×10^{-3}	0	2.837×10^{-4}	1.017×10^{-2}	
Spot Quadrangulated	1474	2928	319	1.174×10^{-3}	3.752×10^{-3}	321	2.221×10^{-3}	1.805×10^{-2}	0	1.882×10^{-3}	8.820×10^{-3}	
Steel Guard -7Mb	3686	0	0	3.056×10^{-4}	8.985×10^{-4}	0	1.779×10^{-4}	2.313×10^{-3}	0	6.544×10^{-4}	1.470×10^{-2}	
Tank	7753	15063	2668	5.878×10^{-4}	3.168×10^{-3}	1819	8.630×10^{-4}	6.261×10^{-3}	0	1.068×10^{-3}	8.947×10^{-3}	
Teacup	2872	5728	1078	5.922×10^{-4}	3.523×10^{-3}	559	9.836×10^{-4}	9.353×10^{-3}	0	1.069×10^{-3}	1.324×10^{-2}	
The Dark Wraith	49951	80572	16367	1.871×10^{-4}	4.231×10^{-3}	7945	3.172×10^{-4}	4.387×10^{-3}	0	3.110×10^{-4}	5.200×10^{-3}	
Venice Mask	74056	35201	5805	2.870×10^{-4}	1.651×10^{-3}	1901	4.972×10^{-4}	4.702×10^{-3}	0	3.605×10^{-4}	2.025×10^{-3}	
Vera Posed	22178	40269	5877	5.464×10^{-4}	4.052×10^{-3}	4038	6.937×10^{-4}	5.271×10^{-3}	0	8.483×10^{-4}	1.379×10^{-2}	
War Tank	15764	27758	4984	7.279×10^{-4}	3.481×10^{-3}	3388	7.236×10^{-4}	1.329×10^{-2}	0	4.366×10^{-3}	2.899×10^{-2}	
Yeahright	188676	377344	93770	5.681×10^{-5}	3.109×10^{-4}	37774	4.919×10^{-5}	9.043×10^{-4}	0	2.998×10^{-5}	7.253×10^{-4}	

10% Reduction			Ours			QEM			MeshLab		
Name	Out Δ	In \square	Out \square	Chamfer ¹	Hausdorff ¹	Out \square	Chamfer ¹	Hausdorff ¹	Out \square	Chamfer ¹	Hausdorff ¹
Door Panel	6471	0	0	3.508×10^{-4}	3.604×10^{-3}	0	6.001×10^{-4}	2.088×10^{-2}	0	4.200×10^{-4}	2.743×10^{-3}
2B	176780	621539	59923	1.658×10^{-4}	1.529×10^{-2}	9406	5.500×10^{-3}	8.592×10^{-2}	0	2.169×10^{-3}	2.911×10^{-3}
Angelica	14858	64994	1834	2.318×10^{-3}	3.814×10^{-2}	2226	3.749×10^{-3}	3.325×10^{-2}	0	1.914×10^{-3}	2.522×10^{-2}
Angkor Wat	48952	0	0	1.481×10^{-4}	2.332×10^{-3}	0	2.690×10^{-4}	1.025×10^{-2}	0	2.152×10^{-4}	3.530×10^{-3}
Arches	2806	14032	1182	5.677×10^{-4}	1.464×10^{-2}	247	4.073×10^{-3}	1.076×10^{-2}	0	5.310×10^{-3}	1.651×10^{-2}
Armadillo	10090	0	0	5.953×10^{-4}	1.900×10^{-3}	0	1.136×10^{-3}	7.254×10^{-3}	0	6.007×10^{-3}	3.457×10^{-3}
Armored Charizard	471	12	12	4.895×10^{-3}	3.601×10^{-2}	12	5.485×10^{-3}	4.389×10^{-2}	0	1.127×10^{-2}	6.829×10^{-2}
Bicycle	12167	41618	2196	5.912×10^{-4}	4.784×10^{-2}	2330	4.959×10^{-4}	7.003×10^{-3}	0	2.208×10^{-3}	1.375×10^{-2}
Blub Quadrangulated	1426	7104	389	8.329×10^{-4}	2.621×10^{-3}	137	1.931×10^{-3}	2.477×10^{-2}	0	1.211×10^{-3}	7.290×10^{-3}
Botchling	31534	157140	11039	2.842×10^{-4}	2.942×10^{-3}	3411	4.792×10^{-4}	3.428×10^{-3}	0	4.000×10^{-3}	3.021×10^{-3}
Casio Keyboard	682	2649	163	2.146×10^{-3}	1.387×10^{-2}	163	1.950×10^{-3}	4.485×10^{-2}	0	1.661×10^{-3}	4.509×10^{-2}
Chimney Pipe	714	3404	235	3.147×10^{-3}	8.976×10^{-3}	123	3.492×10^{-3}	2.293×10^{-2}	0	5.191×10^{-3}	4.793×10^{-2}
Chitinous Knight	17476	87212	5810	3.976×10^{-4}	2.995×10^{-3}	945	6.607×10^{-4}	3.989×10^{-3}	0	5.423×10^{-3}	2.517×10^{-3}
Cube	1018	4236	336	2.307×10^{-3}	3.164×10^{-3}	52	8.905×10^{-3}	1.103×10^{-1}	0	2.912×10^{-2}	1.273×10^{-1}
Cyberpunk Bike	6375	30488	1891	1.172×10^{-3}	1.536×10^{-2}	1114	1.209×10^{-3}	1.166×10^{-2}	0	1.515×10^{-3}	1.195×10^{-2}
Dense Cube	202	1014	93	3.429×10^{-10}	1.517×10^{-9}	12	5.677×10^{-7}	1.562×10^{-5}	0	2.105×10^{-3}	3.316×10^{-2}
Dragon With Pearl	101220	0	0	2.140×10^{-4}	8.429×10^{-4}	0	4.738×10^{-4}	3.016×10^{-3}	0	2.300×10^{-4}	1.500×10^{-3}
Dreadroamer	15182	0	0	8.440×10^{-4}	6.997×10^{-3}	0	1.034×10^{-3}	6.257×10^{-3}	0	1.185×10^{-3}	1.040×10^{-2}
Dry Tree	15242	0	0	1.953×10^{-3}	9.429×10^{-2}	0	4.735×10^{-3}	1.202×10^{-1}	0	9.845×10^{-4}	1.051×10^{-2}
Egyptian Vase	1430	7116	316	1.363×10^{-3}	3.962×10^{-3}	57	1.838×10^{-3}	8.640×10^{-3}	0	2.815×10^{-3}	1.070×10^{-2}
Fandisk	1298	0	0	2.581×10^{-4}	2.468×10^{-3}	0	5.515×10^{-3}	2.452×10^{-2}	0	5.092×10^{-3}	6.444×10^{-4}
Floral Pattern	20976	104752	9180	6.129×10^{-5}	1.047×10^{-3}	1301	6.657×10^{-5}	4.118×10^{-3}	0	1.470×10^{-4}	3.539×10^{-3}
French Halfbasket	7066	35288	3392	1.025×10^{-4}	5.269×10^{-4}	458	9.936×10^{-5}	1.381×10^{-3}	0	2.241×10^{-4}	1.391×10^{-3}
Globophobia	7671	38235	2447	4.932×10^{-4}	1.320×10^{-2}	661	8.700×10^{-4}	5.204×10^{-3}	0	7.158×10^{-4}	1.060×10^{-2}
Goblin Portrait	11008	54388	1762	7.723×10^{-4}	8.097×10^{-3}	880	1.382×10^{-3}	8.175×10^{-3}	0	1.250×10^{-3}	9.116×10^{-3}
Greek Vase	2520	12544	732	1.150×10^{-3}	3.896×10^{-3}	337	3.101×10^{-3}	3.301×10^{-2}	0	2.166×10^{-3}	1.079×10^{-2}
His Name Is Violence	2700	11778	614	2.333×10^{-3}	1.489×10^{-2}	364	2.105×10^{-3}	1.774×10^{-2}	0	4.400×10^{-3}	3.653×10^{-2}
Hover Bike	939	0	0	6.194×10^{-3}	3.323×10^{-2}	0	5.400×10^{-3}	2.478×10^{-2}	0	6.840×10^{-3}	2.381×10^{-2}
Japanese House 2	46964	233904	21572	1.374×10^{-4}	1.412×10^{-3}	9400	1.859×10^{-4}	3.645×10^{-3}	0	6.991×10^{-3}	1.076×10^{-3}
Japanese House 3	8294	41298	2282	9.295×10^{-4}	4.238×10^{-3}	1363	7.680×10^{-4}	1.167×10^{-2}	0	6.551×10^{-4}	7.385×10^{-3}
Japanese Shinto Shrine	1310	5790	472	2.789×10^{-3}	4.795×10^{-2}	388	1.376×10^{-3}	4.030×10^{-2}	0	3.911×10^{-3}	7.180×10^{-2}
Kagiya Edo Tokyo	3450	9855	889	1.531×10^{-3}	1.503×10^{-2}	320	1.534×10^{-3}	2.876×10^{-2}	0	1.927×10^{-3}	5.719×10^{-2}
Lamborghini Countach	26826	119160	3444	4.780×10^{-4}	3.353×10^{-2}	3868	3.224×10^{-4}	1.440×10^{-2}	0	1.930×10^{-3}	4.675×10^{-2}
Lantern	272	1328	84	5.683×10^{-3}	1.480×10^{-2}	68	3.496×10^{-3}	4.947×10^{-2}	0	1.388×10^{-3}	5.030×10^{-2}
Lego Figure	371	0	0	3.840×10^{-3}	1.952×10^{-2}	0	2.986×10^{-3}	2.064×10^{-2}	0	2.264×10^{-3}	2.999×10^{-2}
Lekythos	221	1075	42	6.265×10^{-3}	1.550×10^{-2}	8	7.899×10^{-3}	2.752×10^{-2}	0	9.839×10^{-3}	2.193×10^{-2}
Lethe	897	3986	196	4.691×10^{-3}	1.781×10^{-1}	173	2.339×10^{-3}	2.008×10^{-2}	0	5.248×10^{-3}	3.005×10^{-2}
Marble Track	7044	26461	1002	1.824×10^{-3}	2.042×10^{-2}	971	6.080×10^{-4}	1.487×10^{-2}	0	1.110×10^{-3}	2.737×10^{-2}
Maze 45	7461	37191	3320	2.295×10^{-4}	3.931×10^{-3}	681	2.794×10^{-4}	1.071×10^{-2}	0	1.056×10^{-3}	3.551×10^{-3}
Maze	7465	37191	3222	3.180×10^{-4}	5.151×10^{-3}	801	3.894×10^{-4}	6.815×10^{-3}	0	1.451×10^{-4}	4.883×10^{-3}
Mech	1550	5850	212	3.803×10^{-3}	1.739×10^{-2}	210	3.197×10^{-3}	1.644×10^{-2}	0	5.292×10^{-3}	2.443×10^{-2}
Melon Pallet	9178	45016	1609	9.265×10^{-4}	2.800×10^{-3}	701	8.442×10^{-4}	9.450×10^{-3}	0	6.854×10^{-3}	5.820×10^{-3}
Militech Robot	5309	0	0	2.221×10^{-3}	9.526×10^{-3}	0	1.880×10^{-3}	9.546×10^{-3}	0	2.223×10^{-3}	4.477×10^{-2}
One Angry Dragon Boid	13606	67632	3581	7.260×10^{-4}	2.652×10^{-3}	1042	1.159×10^{-3}	9.430×10^{-3}	0	8.773×10^{-3}	6.936×10^{-3}
Oni No Face Mask	22072	0	0	2.044×10^{-4}	2.480×10^{-3}	0	5.213×10^{-4}	4.911×10^{-3}	0	1.750×10^{-4}	2.288×10^{-3}
Organic Armor	9460	47270	3939	3.127×10^{-4}	1.252×10^{-3}	459	4.088×10^{-4}	2.845×10^{-3}	0	4.127×10^{-4}	2.140×10^{-3}
Pipe Wall	312	1543	59	9.273×10^{-3}	1.297×10^{-1}	40	4.413×10^{-3}	7.112×10^{-2}	0	5.385×10^{-3}	1.278×10^{-1}
Prometheus	80992	379559	27777	1.449×10^{-4}	1.210×10^{-2}	8636	1.733×10^{-4}	1.999×10^{-3}	0	2.211×10^{-4}	2.275×10^{-3}
Radial	1012	0	0	9.064×10^{-3}	4.366×10^{-2}	0	8.057×10^{-3}	5.451×10^{-2}	0	2.482×10^{-3}	8.721×10^{-2}
Roman Soldier	28201	123893	8416	3.586×10^{-4}	2.455×10^{-3}	2372	6.014×10^{-4}	3.994×10^{-3}	0	5.988×10^{-4}	3.418×10^{-3}
Rope Bridge	1234	4444	474	5.797×10^{-3}	4.262×10^{-2}	293	8.610×10^{-4}	4.831×10^{-3}	0	1.103×10^{-3}	2.202×10^{-2}
Shinto Watchtower	26964	123508	10531	1.235×10^{-3}	3.226×10^{-3}	4154	1.275×10^{-3}	8.236×10^{-3}	0	1.902×10^{-3}	1.466×10^{-2}
Shirakawago House	3238	15867	982	3.033×10^{-3}	2.430×10^{-2}	636	4.001×10^{-3}	6.284×10^{-2}	0	4.743×10^{-3}	6.843×10^{-2}
Skyward Ddf Pocco Ship	19831	12207	1519	1.222×10^{-4}	2.718×10^{-3}	653	1.642×10^{-4}	2.935×10^{-3}	0	4.220×10^{-4}	8.469×10^{-3}
Snowflake Orb	7802	0	0	3.618×10^{-3}	7.027×10^{-3}	0	4.045×10^{-3}	2.033×10^{-2}	0	4.113×10^{-3}	1.861×10^{-2}
Space Fighter	7437	34057	2472	6.579×10^{-4}	1.365×10^{-2}	2487	4.859×10^{-4}	2.472×10^{-2}	0	1.161×10^{-3}	1.242×10^{-2}
Speeder Bike	2486	11568	721	1.744×10^{-3}	1.695×10^{-1}	360	1.699×10^{-3}	2.706×10^{-2}	0	2.383×10^{-3}	1.816×10^{-2}
Spiral Staircase	1496	1400	215	1.682×10^{-3}	8.283×10^{-3}	327	7.642×10^{-4}	1.520×10^{-2}	0	8.742×10^{-4}	3.462×10^{-2}
Spot Quadrangulated	602	2928	73	2.744×10^{-3}	8.350×10^{-3}	40	5.393×10^{-3}	3.987×10^{-2}	0	4.828×10^{-3}	1.762×10^{-2}
Steel Guard -7Mb	1490	0	0	1.238×10^{-3}	3.627×10^{-3}	0	5.901×10^{-4}	5.150×10^{-3}	0	7.474×10^{-3}	6.117×10^{-2}
Tank	3148	15063	916	1.715×10^{-3}	9.359×10^{-3}	534	1.951×10^{-3}	1.232×10^{-2}	0	2.382×10^{-3}	1.841×10^{-2}
Teacup	1162	5728	234	1.342×10^{-3}	4.688×10^{-3}	91	2.030×10^{-3}	1.248×10^{-2}	0	2.683×10^{-3}	1.831×10^{-2}
The Dark Wraith	20134	80572	4155	4.387×10^{-4}	4.865×10^{-3}	1676	6.707×10^{-4}	5.159×10^{-3}	0	7.361×10^{-4}	8.545×10^{-3}
Venice Mask	29883	35201	1608	5.726×10^{-4}	4.691×10^{-3}	389	9.735×10^{-4}	7.530×10^{-3}	0	7.487×10^{-4}	4.059×10^{-3}
Vera Posed	8995	40269	1858	1.421×10^{-3}	8.336×10^{-3}	1005	1.464×10^{-3}	1.027×10^{-2}	0	1.943×10^{-3}	1.738×10^{-2}
War Tank	6578	27758	1647	2.413×10^{-3}	2.748×10^{-2}	915	1.953×10^{-3}	3.493×10^{-2}	0	7.018×10^{-3}	3.555×10^{-2}
Yeahright	75484	377344	36959	1.327×10^{-4}	6.005×10^{-4}	6600	1.322×10^{-4}	1.741×10^{-3}	0	1.033×10^{-4}	3.103×10^{-3}
Average				1.811×10^{-3}	1.970×10^{-2}		2.066×10^{-3}				



Fig. 19. Comparison of geometric distance for each of 19 animated models for our approach and “QEM” which implements [Landreneau and Schaefer, 2009]. Our approach consistently outperforms prior work, especially when considering chamfer distance. On each chart, the x-axis indicates the frame of animation when the distance is measured. For both Chamfer and Hausdorff distances, lower on the y-axis indicates more similarity with the original model. ACM Trans. Graph., Vol. 1, No. 1, Article 1. Publication date: January 2024.

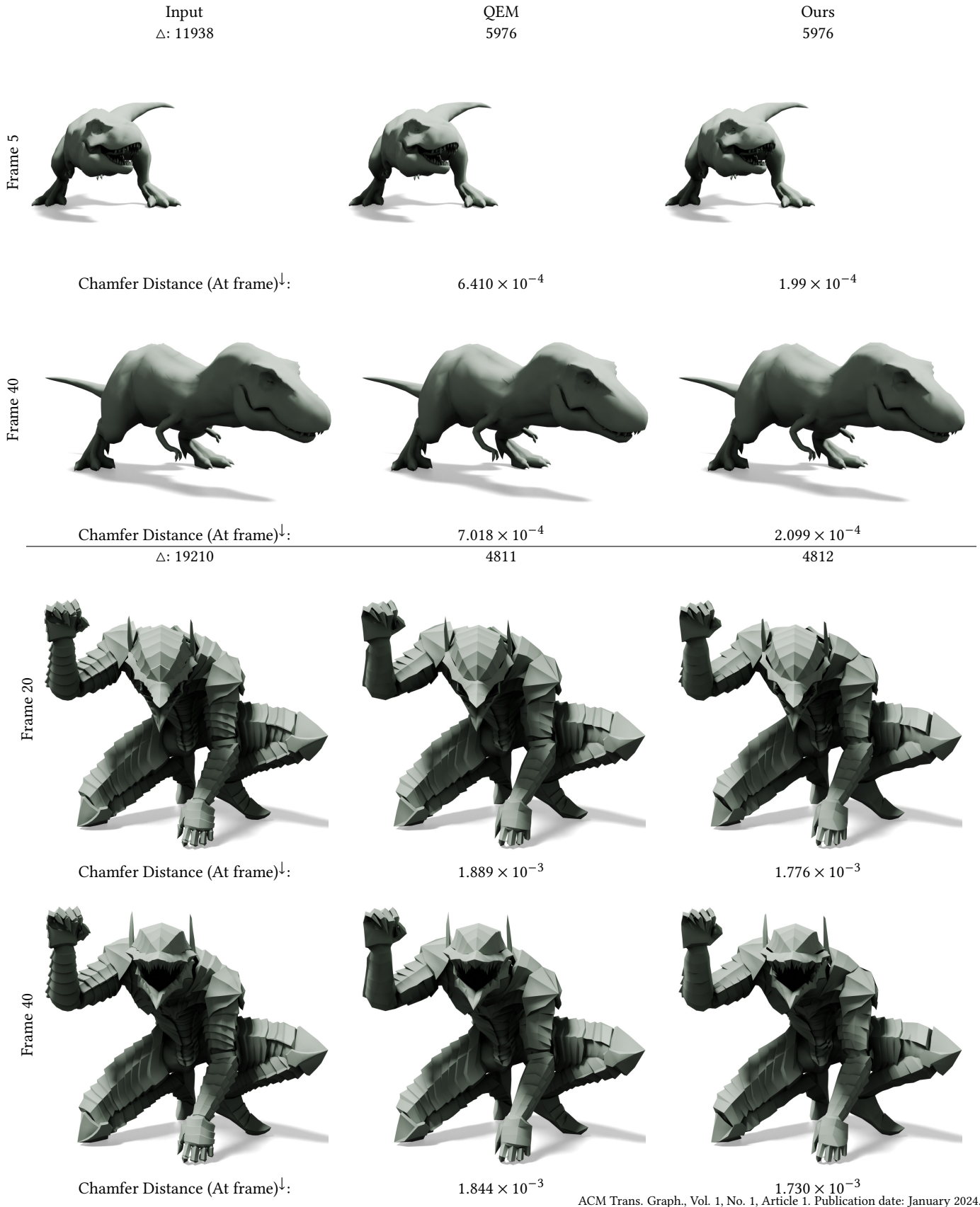


Fig. 20. Visual comparison of our approach against QEM, which implements [Landreneau and Schaefer, 2009], on two animated meshes. For each mesh, the camera is at a single position, but it appears different as the T-rex travels a large distance during animation.